JGR Planets

RESEARCH ARTICLE
10.1029/2019JE006362

Key Points:
- We present an updated catalog of 91 lunar Irregular Mare Patches (IMPs) and survey the geologic settings and characteristics of each IMP
- Two classification schemes for the entire IMP population are proposed on the basis of their geologic settings and characteristics
- The characteristics of lunar IMPs are consistent with the waning-stage magmatic foam extrusion origin model in different environments

Correspondence to:
L. Qiao and Z. Ling,
leqiao.geo@gmail.com;
zcling@sdu.edu.cn

Citation:
Qiao, L., Head, J. W., Ling, Z., & Wilson, L. (2020). Lunar irregular mare patches: Classification, characteristics, geologic settings, updated catalog, origin, and outstanding questions. *Journal of Geophysical Research: Planets*, *125*, e2019JE006362. https://doi.org/10.1029/2019JE006362

Received 29 DEC 2019
Accepted 7 MAY 2020
Accepted article online 28 MAY 2020

©2020. American Geophysical Union. All Rights Reserved.

Lunar Irregular Mare Patches: Classification, Characteristics, Geologic Settings, Updated Catalog, Origin, and Outstanding Questions

Le Qiao[1,2], James W. Head[3], Zongcheng Ling[1], and Lionel Wilson[4]

[1]Shandong Key Laboratory of Optical Astronomy and Solar-Terrestrial Environment, School of Space Science and Physics, Institute of Space Sciences, Shandong University, Weihai, China, [2]Key Laboratory of Lunar and Deep Space Exploration, Chinese Academy of Sciences, Beijing, China, [3]Department of Earth, Environmental and Planetary Sciences, Brown University, Providence, RI, USA, [4]Lancaster Environment Centre, Lancaster University, Lancaster, UK

Abstract One of the most mysterious lunar features discovered during the Apollo era was Ina, a ~2 × 3-km depression composed of bleb-like mounds surrounded by hummocky and blocky terrains. Subsequent studies identified dozens of similar features in lunar maria, describing them as Irregular Mare Patches (IMPs). Due to the unusual and complex characteristics of IMPs, their specific formation mechanism is debated. To improve our understanding of the nature and origin of IMPs, we undertook an updated search and geological characterization of all IMPs and established a classification approach encompassing the full spectrum of IMPs. We present an updated catalog of 91 IMPs and survey the detailed characteristics of each IMP. We find that the majority of IMPs occur in maria emplaced over three billion years ago, contemporaneous with the peak period of global lunar volcanism. We utilized geologic context information and characteristics to establish two classification schemes for lunar IMPs: (1) geologic context: IMPs are categorized into (a) small shield volcano summit pit floor and flank, (b) linear/sinuous rille interior and adjacent exterior, and (c) typical maria; (2) characteristics: IMPs are classified into (a) "mound + floor" and (b) "pit only" types. We showed the range of characteristics of lunar IMPs was consistent with the waning-stage magmatic foam formation and extrusion scenario in different environments. Our updated catalog and classification raise several outstanding questions concerning the nature and origin of lunar IMPs. Assessing these questions will improve our knowledge of lunar thermal and geologic evolution.

Plain Language Summary Composed of fresh-looking bulbous-shaped mounds surrounded by a hummocky and blocky floor, the 2 × 3-km Ina depression is one of the most enigmatic and poorly understood features discovered during early lunar exploration. Later studies identified dozens of similar features in the lunar maria and named them Irregular Mare Patches (IMPs). To achieve an improved knowledge of IMPs, we undertook an updated search, geologic analysis, and classification study of all currently known IMPs, presenting a combined catalog of 91 IMPs. We find that the majority of lunar IMPs occur in mare units emplaced over three billion years ago, coinciding with the peak period of global lunar volcanism. We then classified the entire IMP population on the basis of their geologic settings and characteristics and documented and classified the detailed surface texture of the floor terrains at each IMP site. These new and updated detailed characterization and classification of the entire IMP population provide important new information about their nature and origin. Association with volcanic vent areas and ancient volcanic structures and deposits suggests that late stage volcanic degassing processes during the period of mare volcanism >3 Ga ago should be considered in more detail.

1. Introduction

One of the most unusual lunar surface features discovered and studied during the Apollo era was the Ina feature. It was first identified by Ewen A. Whitaker on Apollo 15 panoramic camera photography (Figure 1b), notable for its unique D-shaped appearance (Whitaker, 1972) and unusual interior structure. This feature had actually been imaged on a pre-Apollo Lunar Orbiter photograph (frame IV-102-H3) but unfortunately missed due to being partially obscured by film processing defects (bi-mat bubbles) (Figure 1a). Subsequent detailed photogeological studies by Farouk El-Baz and his colleagues (El-Baz, 1972, 1973; Evans & El-Baz, 1973; Strain & El-Baz, 1980) informally designated Ina as "D-Caldera"

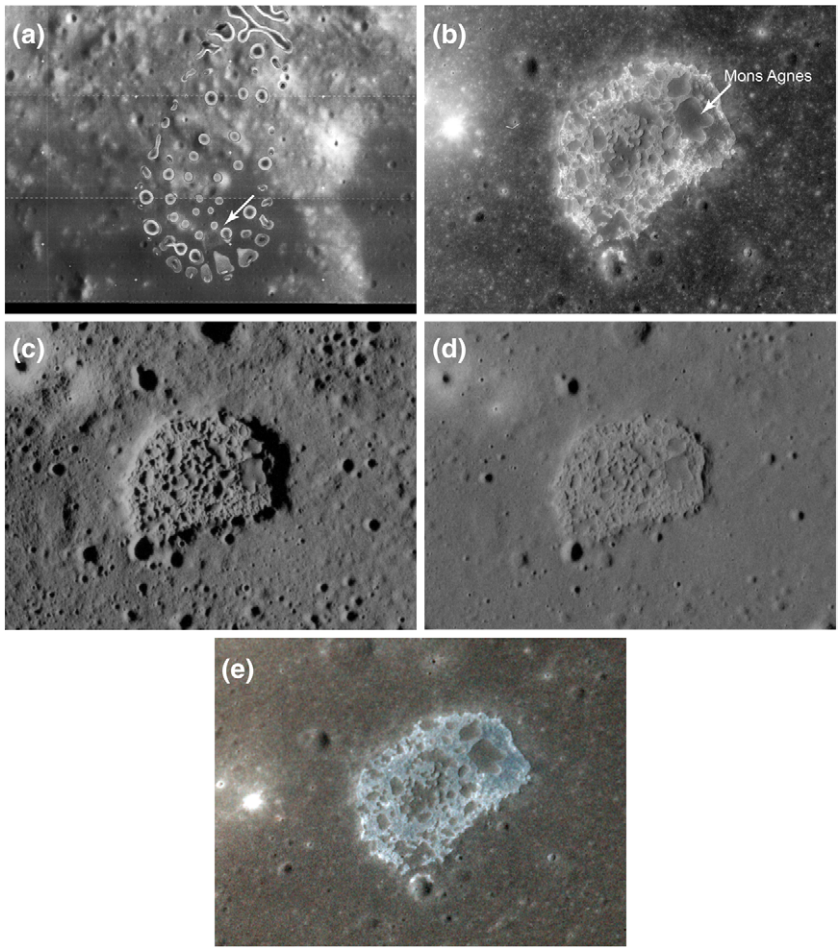


Figure 1. Views of the Ina feature obtained during the Apollo era: (a) Lunar Orbiter photograph, portion of frame IV-102-H3, solar angle (from horizon) 68.4°, Ina feature is pointed out; (b) Apollo 15 panoramic camera photo, portion of frame AS15-P-0181, solar angle 65.0°, Mons Agnes is pointed out; (c) Apollo 17 metric camera photo, portion of frame AS17-M-1518, solar angle 4.0°; (d) Apollo 17 metric camera photo, portion of frame AS17-M-1821, solar angle 13.0°; (e) Apollo 17 color Hasselblad camera (70 mm) photograph, portion of frame AS17–152-23,287, solar angle 46°.

and presented many observations concerning its characteristics and possible mode of origin (Figures 1b–1e). The name "Ina" appeared first in a topophotomap published by NASA in 1974 (sheet 41C3S1(10)) and was then approved by the International Astronomical Union in 1979, along with the nomenclature *Mons Agnes* for the major mound at the eastern interior floor margin (Figure 1b).

Reanalyses of Apollo imaging data sets found that Ina-like features were not unique; similar but much smaller depressions were identified having reflective, rubbly floors bounded by irregular, highly reflective scarps in three locations: (1) on the floor of Hyginus crater (Schultz, 1976; 7.726°N, 6.350°E), (2) along the extension of a graben in SW Mare Tranquillitatis (Schultz, 1976; 4.096°N, 21.218°E), and (3) along the western edge of Mare Serenitatis (Masursky et al., 1978; a group of small depressions at 24.773°N, 8.045°E, Aratus D-1 to 3 in Table 2). Newly acquired submeter-scale Lunar Reconnaissance Orbiter Narrow Angle Cameras (LROC NAC) images enable the identification of dozens of new features on mare surfaces with similar morphologies. Stooke (2012) initiated this campaign and found 23 additional Ina-like features (termed "meniscus hollows") in several mare locations: west edge of Mare Serenitatis ($n = 3$; near to those found in Masursky et al., 1978), NW Mare Tranquillitatis ($n = 7$), West Mare Fecunditatis ($n = 6$), northern margin of Mare Insularum ($n = 4$), SW corner of Mare Imbrium ($n = 1$), the vicinity of a rille in Oceanus Procellarum

Table 1
Previous Theories for the Origin of Lunar IMPs and the Associated Deposits

IMP origin theory	Reference	Interpretation of the associated deposits of lunar IMPs.
Sublimation[a]	Whitaker, 1972	Mounds: mare-like materials; floor terrain: potential sublimates.
Small lava intrusions within a collapse caldera atop an extrusive volcanic dome	El-Baz, 1972, 1973; Strain & El-Baz, 1980	Entire Ina structure: summit caldera; mounds: small lava intrusions (among the youngest volcanism on the Moon, but age not specifically determined).
Removal of surface regolith by episodic out-gassing within the past 10 Ma	Schultz et al., 2006	Exposure of long-buried ancient (>3.5 Ga) high-titanium mare basalts.
Lava flow inflation	Garry et al., 2012	Mounds: inflated lava flows; floor hummocky terrains: lava breakouts; blocky units: mass wasting exposures.
Small basaltic eruptions within the past 100 Ma	Braden, 2013; Braden et al., 2014	Mounds: small magma extrusions; floor units: disrupted lava pond crust.
Possible pyroclastic eruption (explains only Cauchy-5 IMP, not Ina)[a]	Carter et al., 2013	Pyroclastic deposits.
Lava lake processes and magmatic foam extrusion	Qiao et al., 2017; Qiao, Hear, Xiao, et al., 2018; Qiao, Head, Ling, Wilson, Xiao, et al., 2019; Wilson & Head, 2017b	Floor hummocky and blocky units: solidified macrovesicular lava lake crust; mounds: solidified magmatic foams.

[a]Symbol denotes relatively simplified origin theories that are deduced from general observations of one parameter.

($n = 1$), and eastern margin of Sinus Aestuum ($n = 1$). Braden et al. (2014) pursued this work and expanded the inventory to 70 features in mare regions in the central nearside of the Moon and described them as irregular mare patches (IMPs). Moreover, several ensuing lunar morphological investigations found additional sporadic IMP occurrences (e.g., Zhang et al., 2018).

1.1. Theories for the Origin of IMPs

Half acentury after the discovery of Ina (the most notable IMP feature) during the Apollo era, the mechanisms of origin, mode of emplacement and age (either ancient or geologically very recent) of IMPs are still being debated (e.g., Braden et al., 2014; El-Baz, 1973; Garry et al., 2012; Qiao et al., 2017; Qiao, Head, Xiao, et al., 2018; Qiao, Head, Ling, Wilson, Xiao, et al., 2019; Schultz et al., 2006; Strain & El-Baz, 1980). A summary of these previously proposed theories for the origin of lunar IMPs and their associated deposits is outlined in Table 1, and more comprehensive details can be found in the references indicated and in Qiao, Head, Ling, Wilson, Xiao, et al. (2019). These prior investigations have documented substantial observations of lunar IMPs, including geologic settings, topography, morphology, morphometry, optical reflectance and maturity, composition from visible, near-infrared, and thermal-infrared spectroscopy, thermophysical properties, surface physical properties, photometry and superposed impact crater populations, and their constraints on previously proposed mechanisms of origin (e.g., Bennett et al., 2015; Braden et al., 2014; Donaldson Hanna et al., 2016; Elder et al., 2017; Garry et al., 2012; Garry et al., 2013; Glaspie et al., 2019; Grice et al., 2016; Neish et al., 2017; Qiao et al., 2017; Qiao, Head, Ling, Wilson, Xiao, et al., 2019; Qiao, Head, Xiao, et al., 2018; Strain & El-Baz, 1980; and references therein).

These substantial observational results and many different and competing theories (Table 1) have raised a line of key questions concerning the nature and origin of lunar IMPs. (1) What is the origin of the various floor terrain textures? (2) What is the thickness and variability of the surface regolith layer? (3) What is the reason for the anomalous surface immaturity? (4) How are the relatively steep walls and slopes maintained? (5) How do the mineralogy and composition compare with those of surrounding units? (6) What are their ages and the causes, including (6a) what is the emplacement age of the deposits of lunar IMPs? (6b) what is the age relationship between mounds and floor units? (6c) how do the ages derived from impact crater size-frequency distributions (CSFDs) compare with those of surrounding units?

Among the major difficulties in resolving the origin of IMPs are their highly variable characteristics and geological settings, both between different IMP occurrences and among different parts of some specific IMP features. Apollo era analyses had already noted the major morphological variations of Ina floor

terrains, including bright rough-textured units, polygonal hummocks, and dark hilly terrains (Strain & El-Baz, 1980). Updated LROC NAC-based morphological investigations documented substantial new textural properties of the floor of Ina, for example, pitted, ridged, polygonal, and vermicular textures (Qiao, Head, Ling, Wilson, Xiao, et al., 2019). In addition, apart from several major IMP occurrences (e.g., Ina, Sosigenes, Cauchy-5, and Hyginus), the detailed geological characteristics of the majority of lunar IMPs, including geologic setting, geomorphology, morphometry, and surface texture, were not well documented. Earlier inspections based on Apollo photographs had revealed the similarity in morphology between Ina and other IMP features, while also noting the apparent differences. For example, the IMPs identified in three other locations are more than one order of magnitude smaller than the Ina feature (maximum length: 40–170 m vs. 2.9 km) and lack the raised mounds observed at Ina (Schultz, 1976, 1991). Recent preliminary analyses using LROC NAC images also noted the wide range of dimensions, structures, and characteristics of the documented IMPs (e.g., Braden et al., 2014; Qiao, Head, Ling, & Wilson, 2019). In order to develop an improved understanding of the formation mechanism of the entire catalogued IMP population, it is necessary to conduct a thorough geological characterization of all the IMP occurrences and to establish classification schemes that take into account the full spectrum of characteristics of lunar IMPs.

In this contribution, we first present an updated, comprehensive catalog of IMP occurrences on the basis of their identification from multiple prior studies. In order to understand the catalogued IMP population as a whole, we analyze the detailed geological characteristics of each IMP feature, including geologic setting, surface model age of the background mare unit, structure, geomorphology, and surface texture. We then develop two IMP classification schemes that illustrate the spectrum of the geologic settings and characteristics of lunar IMPs and their variations. We also investigate the applicability of the waning-stage magmatic foam formation and extrusion scenario to the origin mechanism of our catalogued IMPs of various categories. We outline several outstanding questions raised by our characterization and classification schemes that need to be explained to understand the origin of IMPs and the constraints they place on the thermal and geologic evolution of the Moon.

2. Data and Methods

We first present an updated catalog of lunar IMPs by compiling multiple previous IMP identification studies, from Apollo era investigations (Schultz, 1976; Whitaker, 1972) to recent LROC NAC image-based surveys (e.g., Braden et al., 2014; Stooke, 2012). We then analyze the geologic setting of each IMP occurrence, including the morphology, topography, and tectonic setting, using the latest moderate-resolution images from the LROC Wide-Angle Camera (WAC, 100 m/pixel, Robinson et al., 2010) and Kaguya Terrain Cameras (TC, 10 m/pixel, Haruyama et al., 2008), and altimetric data from the Kaguya TC stereogrammetry digital terrain model (DTM) (10-m pixel size and ~3- to 4-m altimetric accuracy; Haruyama et al., 2012; Barker et al., 2014) and Kaguya TC + LRO-LOLA (Lunar Orbiter Laser Altimeter) merged topography (SLDEM2015; 512 pixels/degree spatial sampling and ~3- to 4-m vertical altimetric accuracy; Barker et al., 2016). We also examine the detailed morphology, morphometry, and surface texture of each IMP feature using high-resolution LROC NAC images (up to 0.47 m/pixel, Robinson et al., 2010). Each individual LROC NAC frame has been preprocessed from the raw NAC EDR (experiment data record) image through photometric correction and map projection using the USGS's Integrated Software for Imagers and Spectrometers (ISIS3; e.g., Anderson et al., 2004) according to the terms of the LROC EDR Data Products Software Interface Specification (Bowman-Cisneros, 2010). When high-resolution LROC NAC DTM topography (2–5 m/pixel and better than 2-m relative horizontal and vertical precision, Henriksen et al., 2017) is available (for 28 IMPs), the detailed topographic characteristics of these IMPs are also analyzed.

3. An Updated IMP Catalog of 91 IMPs

We synthesize IMP occurrences from multiple sources beginning with the Apollo era investigations, namely, earlier identifications by Whitaker (1972), Schultz (1976), and Masursky et al. (1978), the LROC NAC-based Stooke catalog (Stooke, 2012), the Braden (2013) and Braden et al. (2014)catalog, two identifications by the recent work Zhang et al. (2018), and several identifications by amateur scientists from THE MOON wiki site (https://the-moon.us/wiki/Irregular_Mare_Patches_(IMPs)) (Tables 2 and 3). Each reported IMP

Journal of Geophysical Research: Planets

10.1029/2019JE006362

Table 2
List of the 21 IMPs Additional to the Braden et al. (2014) Catalog

Informal name	Max. length (m)	Lat (°)	Lon (°)	Host mare	Geologic context	IMP characteristics	Source reference
Al-Bakri-1	660	13.952	20.044	Tranquillitatis	Mare plain	Rough, bright and pitted surface within mare plain	Moon-Wiki site
Arago N	60	7.586	21.019	Tranquillitatis	Mare plain; 1.3 km NE of #10 IMP in Braden et al. (2014) catalog	Rough, bright and pitted surface within mare plain	Braden, 2013
Aratus D-2	100	24.757	7.995	Serenitatis	Mare volcanic edifices	Quasi-circular, rough and bright pits within mare plain	Masursky et al., 1978; also #14 in Stooke, 2012
Aratus D-3	70	24.726	8.069	Serenitatis	Mare plain	Quasi-circular, rough and bright pits within mare plain	Masursky et al., 1978; also #14 in Stooke, 2012
Aratus D-4	90	24.534	8.065	Serenitatis	Mare plain	Irregular rough and bright pits at the upper wall of a circular depression	Stooke, 2012, #16
Aratus D-5	150	24.497	8.130	Serenitatis	On the wall and rim of a linear rille	Irregular and arched rough pits at the upper wall and rim of a circular depression	Stooke, 2012, #14
Aratus D-6	15	24.370	8.117	Serenitatis	Mare plain	Small, quasi-circular rough pits at the upper wall of a circular depression	Stooke, 2012, #15
Bessarion V-1	660	14.917	−33.7	Insularum	Mare structures; in an area with a cluster of IMPs including #27, #51,and #64 IMPs in Braden et al. (2014) catalog	Rough, bright pits with ridged, vermicular features on the floors	Stooke, 2012, #24
Bessarion V-2	150	14.839	−33.876	Insularum	Mare structures; in an area with a cluster of IMPs including #27, #51, and #64 IMPs in Braden et al. (2014) catalog	Rough, bright pits at the upper wall and rim of a circular depression	Stooke, 2012, #27
Bessarion V-3	200	14.55	−33.856	Insularum	Slope of mare structures; in an area with a cluster of IMPs including #27, #51, and #64 IMPs in Braden et al. (2014) catalog	Rough, bright pits at slopes	Moon-Wiki site
Bessarion V-4	130	14.267	−33.566	Insularum	Mare plain; in an area with a cluster of IMPs including #27, #51 and #64 IMPs Braden et al. (2014) catalog	Rough, bright pits at the upper wall of a circular depression	Moon-Wiki site
Boda E-1	50	13.089	−3.760	Sinus Aestuum	Mare plain; 5 km north of #50 IMP in Braden catalog	Irregular rough and bright pits at the upper wall of a circular depression	Stooke, 2012, #11
Brayley D	30	19.145	−32.579	Imbrium	On the rim of a quasi-elliptic vent	Elliptic, rough and bright pit on the rim of a vent	Stooke, 2012, #13
Maclear-4	320	10.597	20.944	Tranquillitatis	Mare plain; between #17 and #31 IMPs in Braden et al. (2014) catalog	Arc-shaped, rough, bright pit within mare plain	Moon-Wiki site
Maclear-5	120	10.603	20.9	Tranquillitatis	Mare plain; between #17 and #31 IMPs in Braden et al. (2014) catalog	Elongated, rough, bright pit within mare plain	Moon-Wiki site
Maclear-6	500	9.283	20.766	Tranquillitatis	Small shield volcano flank; 1.7 km NW of the Arago-5 IMP in the Braden et al., 2014 catalog	Rough and pitted surface	Moon-Wiki site
Secchi X-1	80	−0.289	42.800	Fecunditatis	Mare plain	Elongated, rough and bright pits at the wall of a very shallow depression	Stooke, 2012, #18
Secchi X-3	20	−0.339	42.804	Fecunditatis	Mare plain	Irregular, rough and bright pits at the wall of a very shallow depression	Stooke, 2012, #19
Secchi X-4	90	−1.883	43.176	Fecunditatis	Mare plain; 6 km NW of #28 IMP in Braden et al. (2014) catalog	Irregular, rough and bright pit	Zhang et al., 2018
Secchi X-5	25	−2.058	43.525	Fecunditatis	Mare plain; 1.5 km north of #62 IMP in Braden et al. (2014) catalog	Irregular rough and bright pits at the upper wall of a circular depression	Stooke, 2012, #21
Vera	70	26.342	−43.76	Oceanus Procellarum	Volcanic vent floor	Elongated, rough and bright pit	Zhang et al., 2018

Table 3
List of 91 IMPs and Their Characteristics and Classifications

#[a]	Name	Max. Length (m)	Lat (°)	Lon (°)	Context class[b]	Characteristics class[c]	Floor terrain texture[d]	Host mare	Host mare age (Ga)	Citation[e]
1	Sosigenes	5,000	8.335	19.071	3	1	1234567	Tranquillitatis	3.68	B14
2	Ina	3,000	18.65	5.3	1	1	1234567	Lacus Felicitatis	3.54	B14
3	Cauchy-5	3,000	7.169	37.592	12	1 + 2A + 2B	1278	Tranquillitatis	3.62	B14
4	Maskelyne	3,000	4.33	33.75	1	1 + 2A + 2B	23478	Tranquillitatis	3.62	B14
5	Nubium	2000	−25.72	−27.681	34	1 + 2A + 2B	2378	Nubium	3.63	B14
6	Ross-E-1	1,200	10.46	23.547	5B	2A	2378	Tranquillitatis	3.68	B14
7	Maclear-2	800	9.102	20.298	5A	2A	2347	Tranquillitatis	3.68	B14
8	Aristarchus North	800	25.044	−46.767	5B	2A + 2B	23467	Oceanus Procellarum	1.2	B14
9	Arago-5	750	9.23	20.824	2	2A	134	Tranquillitatis	3.68	B14
10	Unnamed	670	7.559	20.984	5B	2A	237	Tranquillitatis	3.68	B14
11	Jansen-1	600	11.669	32.659	5A	2A + 2B	237	Tranquillitatis	3.57	B14
12	Unnamed	560	8.298	21.6	5A	2A + 2B	237	Tranquillitatis	3.68	B14
13	Unnamed	550	9.58	25.514	5A	2A	237	Tranquillitatis	3.68	B14
14	Unnamed	500	7.348	20.897	5A	2A	1237	Tranquillitatis	3.68	B14
15	Maclear-1	430	8.891	21.487	5A	2A	237	Tranquillitatis	3.68	B14
16	Unnamed	400	9.112	21.758	5A	2A	278	Tranquillitatis	3.68	B14
17	Unnamed	400	10.31	21.36	5A	2A	237	Tranquillitatis	3.68	B14
18	Unnamed	350	8.67	17.51	5A	2A	123467	Tranquillitatis	3.68	B14
19	Unnamed	350	9.564	25.392	5A	2A	237	Tranquillitatis	3.68	B14
20	Unnamed	350	9.432	26.287	1	2B	234	Tranquillitatis	3.68	B14
21	Unnamed	350	21.653	−0.865	4	2A	2347	Imbrium		B14
22	Unnamed	340	9.54	20.22	5A	2A	237	Tranquillitatis	3.68	B14
23	GEM30	330	37.919	−45.221	5B	2A	237	Unnamed		B14
24	Unnamed	315	7.887	21.937	5A	2A	237	Tranquillitatis	3.68	B14
25	Jansen-2	300	11.235	32.806	5A	2A + 2B	237	Tranquillitatis	3.57	B14
26	Unnamed	300	10.163	19.228	5A	2A	237	Tranquillitatis	3.68	B14
27	Unnamed	300	14.44	−33.656	5B	2B	89	Insularum	2.12	B14
28	GEM1	300	38.152	−44.6	5B	2A	237	Unnamed		B14
29	Unnamed	280	10.045	25.247	5A	2A + 2B	378	Tranquillitatis	3.68	B14
30	Manilus-1	270	14.889	6.467	3	2A	2378	Vaporum	3.23	B14
31	Unnamed	270	10.77	20.52	5A	2A	278	Tranquillitatis	3.68	B14
32	Unnamed	255	9.102	20.265	5A	2A	237	Tranquillitatis	3.68	B14
33	Unnamed	250	9.894	24.851	5B	2A	237	Tranquillitatis	3.68	B14
34	Unnamed	250	37.121	−40.626	5A	2A	378	Imbrium		B14
35	Unnamed	230	8.279	9.319	5B	2A + 2B	237	Vaporum	3.73	B14
36	Carrel-1	200	9.817	25.519	5A	2A + 2B	2378	Tranquillitatis	3.68	B14
37	Manilus-2	200	14.628	6.821	1	2B	8	Vaporum	3.23	B14
38	Unnamed	200	9.244	23.924	5A	2A	2378	Tranquillitatis	3.68	B14
39	GEM24	200	37.428	−43.543	5A	2A	78	Unnamed		B14
40	GEM4	190	38.09	−44.584	5B	2A	378	Unnamed		B14
41	GEM28	175	37.304	−43.628	5A	2B	278	Unnamed		B14
42	Unnamed	170	4.096	21.218	5A	2A	378	Tranquillitatis	3.71	B14
43	GEM3	170	38.115	−44.677	5B	2A	23478	Unnamed		B14
44	Unnamed	160	8.844	21.762	5A	2A + 2B	2378	Tranquillitatis	3.68	B14
45	Unnamed	160	13.131	−4.361	4	2B	2378	Sinus Aestuum		B14
46	Hyginus	150	7.726	6.35	3	2A + 2B	2378	Vaporum	3.73	B14
47	Unnamed	150	7.083	38.574	5A	2A	378	Tranquillitatis	3.62	B14
48	Unnamed	150	8.714	19.383	5A	2B	28	Tranquillitatis	3.68	B14
49	Unnamed	150	10.101	25.278	5A	2A	378	Tranquillitatis	3.68	B14
50	Unnamed	150	12.931	−3.806	4	2B	189	Sinus Aestuum		B14
51	Unnamed	150	14.597	−33.979	5B	2A + 2B	78	Insularum	2.12	B14
52	GEM21	150	37.882	−44.288	5B	2B	2789	Unnamed		B14
53	GEM32	140	37.826	−45.129	5B	2A	237	Unnamed		B14
54	GEM7	140	38.058	−44.073	5A	2B	78	Unnamed		B14
55	Unnamed	130	4.55	22.882	5A	2A + 2B	2478	Tranquillitatis	3.58	B14
56	Unnamed	130	2.934	38.975	5A	2A + 2B	78	Tranquillitatis	3.5	B14
57	GEM11	130	37.941	−44.218	5B	2B	89	Unnamed		B14
58	Unnamed	125	−2.008	43.333	5A	2B	278	Fecunditatis	3.47	B14

Table 3
Continued

#[a]	Name	Max. Length (m)	Lat (°)	Lon (°)	Context class[b]	Characteristics class[c]	Floor terrain texture[d]	Host mare	Host mare age (Ga)	Citation[e]
59	GEM 31	120	38.018	−44.113	5A	2B	78	Unnamed		B14
60	Unnamed	100	9.012	22.248	5B	2A	78	Tranquillitatis	3.68	B14
61	Unnamed	100	9.738	22.32	5B	2A	78	Tranquillitatis	3.68	B14
62	Unnamed	100	−2.113	43.512	5A	2B	78	Fecunditatis	3.47	B14
63	Unnamed	100	26.786	−42.959	4	2A + 2B	34678	Oceanus Procellarum	3.48	B14
64	Unnamed	100	14.468	−33.729	5B	2A + 2B	9	Insularum	2.12	B14
65	GEM35	100	36.937	−44.121	5B	2B	378	Unnamed		B14
66	GEM29	100	37.904	−45.08	5B	2A	2378	Unnamed		B14
67	GEM26	100	37.417	−43.577	5A	2A	78	Unnamed		B14
68	GEM17	100	37.974	−44.285	5B	2B	78	Unnamed		B14
69	GEM12	100	37.995	−44.159	5A	2B	78	Unnamed		B14
70	GEM6	100	37.864	−44.478	5B	2A + 2B	78	Unnamed		B14
71	Al-Bakri-1	660	13.952	20.044	5A	2A + 2B	237	Tranquillitatis	3.68	MW
72	Arago N	60	7.586	21.019	5B	2A + 2B	78	Tranquillitatis	3.68	B13
73	Aratus D-2	100	24.757	7.995	5B	2A + 2B	48	Serenitatis	3.3	M78, S12
74	Aratus D-3	70	24.726	8.069	5A	2A	478	Serenitatis	3.3	M78, S12
75	Aratus D-4	90	24.534	8.065	5A	2B	78	Serenitatis	3.3	S12
76	Aratus D-5	150	24.497	8.130	4	2A	78	Serenitatis	3.3	S12
77	Aratus D-6	15	24.370	8.117	5A	2B	78	Serenitatis	3.3	S12
78	Bessarion-V-1	660	14.92	−33.7	5B	2A + 2B	247	Insularum	2.12	MW
79	Bessarion-V-2	150	14.84	−33.885	5B	2A + 2B	78	Insularum	2.12	MW
80	Bessarion-V-3	200	15.56	−33.86	5B	2B	89	Insularum	2.12	MW
81	Bessarion-V-4	130	14.27	−33.57	5A	2B	78	Insularum	2.12	MW
82	Boda E-1	50	13.089	−3.760	5A	2B	78	Sinus Aestuum		S12
83	Brayley D	30	19.145	−32.579	4	2A	78	Imbrium	2.12	S12
84	Maclear-4	320	10.6	20.94	5A	2A	278	Tranquillitatis	3.68	MW
85	Maclear-5	120	10.604	20.9	5A	2A	78	Tranquillitatis	3.68	MW
86	Maclear-6	500	9.283	20.766	2	2A	238	Tranquillitatis	3.68	MW
87	Secchi X-1	80	−0.289	42.800	5A	2B	78	Fecunditatis	3.53	S12
88	Secchi X-3	20	−0.339	42.804	5A	2B	78	Fecunditatis	3.53	S12
89	Secchi X-4	90	−1.882	43.176	5A	2A	7	Fecunditatis	3.47	S12
90	Secchi X-5	25	−2.058	43.525	5A	2B	78	Fecunditatis	3.47	S12
91	Vera	70	26.342	−43.76	3	2A	78	Oceanus Procellarum	3.48	Z18

[a] #1–70 IMPs are those listed in the tab. S1 of Braden et al., (2014), others are additional IMPs in Table 2. [b] Lunar IMP geologic context class: small shield volcano summit pit floor (Context #1) and flank (Context #2), pit crater chain or linear/sinuous rille interior (Context #3) and adjacent exterior (Context #4), and typical mare deposits (Context #5A: mare plain and Context #5B: mare features and structures), a multiple-digital number indicates a combination of the multiple classes, e.g., "12" means this IMP contains both Types #1 and #2 geologic settings (same for characteristics class and floor terrain texture encodings). [c] Lunar IMP characteristic class: mound + floor type (Class #1) and "pit only" type (Class #2A: within maria and Class #2B: associated with depressions). [d] Floor terrain texture types: (1) smooth terrain, (2) hummocky, (3) pitted, (4) ridged, (5) polygonal, (6) vermicular, (7) blocky, (8) uneven, and (9) bright streak. [e] Citation: source reference for IMP identifications, B13: Braden, 2013, B14: Braden et al., 2014, M78: Masursky et al., 1978, S12: Stooke, 2012, MW: THE MOON wiki site and Z18: Zhang et al., 2018. Note some identifications by Braden et al., (2014) have been previously reported (see their table S1).

occurrence has been visually checked and confirmed on meter-scale LROC NAC images. In total, our updated catalog includes 91 IMPs (Figure 2 and Table 3). IMPs identified in addition to the population in the Braden et al. (2014) catalog are listed in Table 2, and illustrative NAC images are shown in Figure 3. Several previously reported IMP identifications are not catalogued here because of their poor resolution on NAC images (either due to their small size or the relatively coarser available NAC image spatial resolution). Of the 21 additional IMPs, 11 are smaller than 100 m (note that Braden et al. (2014) only listed IMP occurrences larger than 100 m).

4. General Characterization of all IMPs

Prior documentation had shown the widespread distribution of IMPs across many nearside maria (Braden et al., 2014), and our updated catalog further expands the known IMP occurrences into two additional

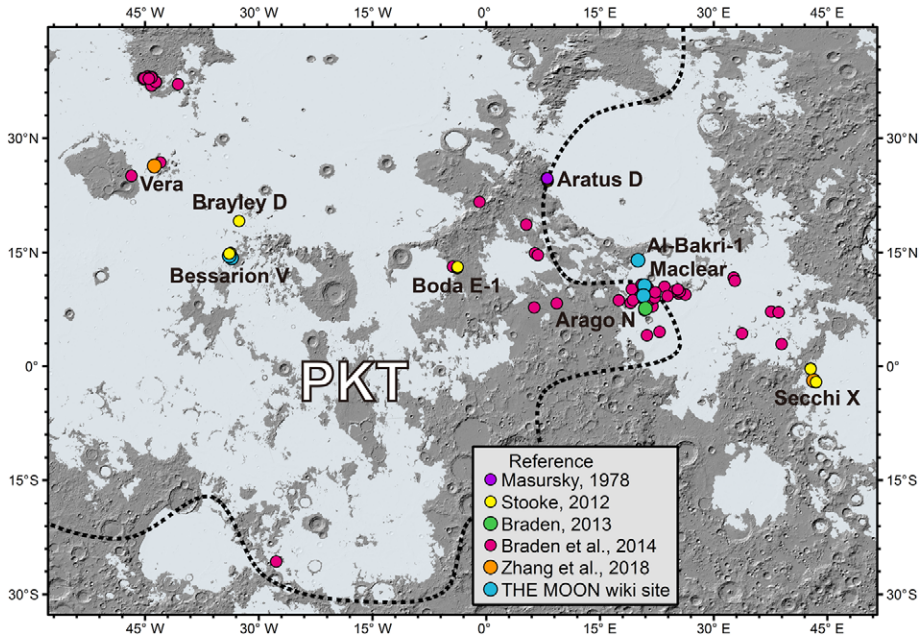


Figure 2. Spatial distribution map of the updated IMP population from several references (see the legend in the bottom). The 21 IMPs additional to the Braden et al. (2014) catalog are labeled (Table 2). Basemap is a hillshade (315° azimuth and 45° altitude) rendering of LOLA 128 pixel/degree topography; exposed mare basalts mapped by Nelson et al. (2014) are shown in white. The boundary of the Procellarum KREEP Terrane (PKT) is delineated by the dashed white line, which is defined by the thorium 3.5-ppm contour line based on the criteria established by Jolliff et al. (2000). The projection is simple cylindrical centered at 0°E, 0°N, and north is up (the same in Figures 5, 6, and 13).

nearside basin-filling maria: Mare Serenitatis (Aratus D IMPs) and Mare Imbrium (Brayley D IMP) (Figure 2). The most concentrated region of IMPs is in western Mare Tranquillitatis (35 IMPs); though not entirely within the Procellarum KREEP Terrane (PKT; Jolliff et al., 2000), this region is characterized by a regional enrichment of thorium abundance (~3–5 ppm; Lunar Prospector Gamma-Ray Spectrometer 0.5° thorium data deconvolved by Lawrence et al., 2003). Another IMP-concentrated region (18 IMPs) near Gruithuisen E and M craters (within PKT) also shows regionally elevated thorium content (~8.5–9.5 ppm). The reason for the presence of small clusters of IMPs in particular mare locations is uncertain from the available observations and analyses. The west Mare Tranquillitatis region displays many NNE-SSW-trending graben and wrinkle ridges, which appear to be concentric to the Tranquillitatis basin center (Yue et al., 2015). Six small shield volcanoes are also observed in this region (Head & Gifford, 1980). The Gruithuisen E and M region contains a group of small mare basaltic deposits scattered on the feldspathic ejecta from the Iridum crater. This area is adjacent to the Gruithuisen silicic domes (6–120 km; Ivanov et al., 2016) and some sinuous rilles (14–75 km), including Rima Sharp, the longest sinuous rille on the Moon (Hurwitz et al., 2013). It is unknown whether the concentration of lunar IMPs in these regions is related to these observed structures. A synthetical analysis of the regional geological context and tectonic setting, topography, morphology, composition (iron, titanium, thorium, etc.), and the association between various geologic features (mare domes, sinuous rilles, wrinkle ridges, graben, etc.) will potentially shed light on this issue.

The identified IMPs are observed to vary in their longest dimension, spanning over one order of magnitude (ranging from <100 m to 5 km; Table 3). Smaller IMPs are more common, with 78% ($n = 71$) of IMPs less than 400 m and 51% ($n = 47$) of IMPs less than 200 m (Figure 4a).

The host mare units of 55 IMPs have been dated through the superposed impact CSFD method (see sources in Figure 5 caption), and 14 IMPs are located in undated mare units, while adjacent to other dated mare units (Table 3). In total, 69 IMPs are located in or near 17 CSFD-dated mare units (Figures 4b and 5). Most of the 69 IMPs ($n = 60$, 87%) are observed to be hosted in mare units that were emplaced between 3.0 and 3.73 Ga ago, contemporaneous with the peak of global lunar volcanism, between ~3.3 and 3.8 Ga ago (313 among the 482

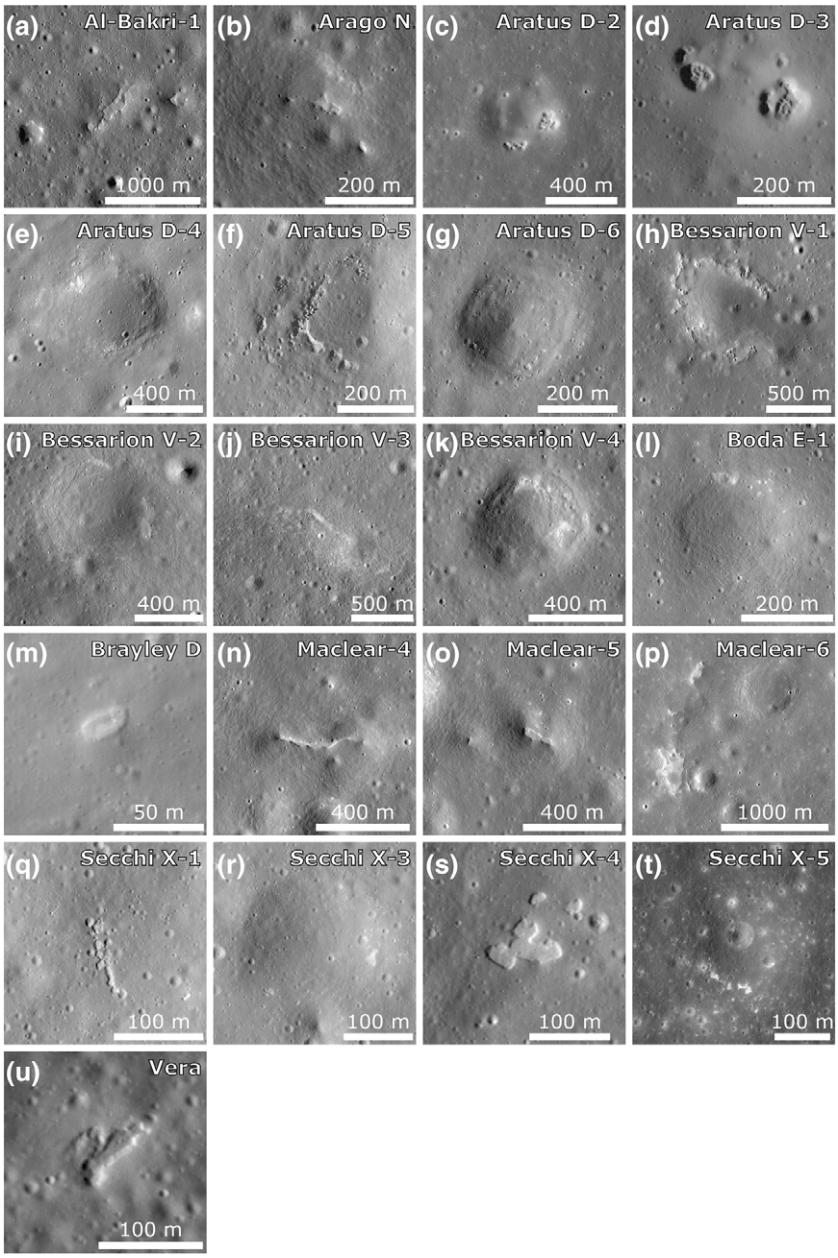


Figure 3. LROC NAC images of the 21 IMPs added to the Braden et al. (2014) catalog: (a) Al-Bakri-1 (the informal name corresponds to that in Table 2), NAC frame M1127000272R, 1.15 m/pixel, 73.71° incidence angle (*i*); (b) Arago N, LROC NAC frame M1096358215L, 1.16-m pixel size, 71.06° incidence angle; this IMP is ~1.3 km NE of the #10 IMP in the Braden et al., 2014 catalog; (c) Aratus D-2, NAC frame M104469044R, 1.45 m/pixel, $i = 57.64°$; (d) Aratus D-3, NAC frame M1218899889L, 1.03 m/pixel, $i = 69.50°$; (e) Aratus D-4, NAC frame M1200072847L, 1.11 m/pixel, $i = 68.24°$; (f) Aratus D-5, NAC frame M150464022L (also for panel g), 0.47 m/pixel, $i = 64.01°$; (g) Aratus D-6; (h) Bessarion V-1, NAC frame M1123818323L, 1.22 m/pixel, $i = 71.34°$; (i) Bessarion V-2, NAC frame M1123818323R (also for panel j), 1.22 m/pixel, $i = 71.35°$; (j) Bessarion V-3; (k) Bessarion V-4, NAC frame M1173279016L, 1.19 m/pixel, 70.16° incidence angle; the Bessarion V IMPs (#1–4), along with three IMPs identified in the Braden et al., 2014 catalog (#27, #51, and #64), occur in a ~20 × 13-km area ~31 km west of the Bessarion V crater in northern margin of Mare Insularum; (l) Boda E-1, NAC frame M150545226L, 0.47 m/pixel, $i = 61.73°$; this IMP is 5 km north of #50 IMP in Braden et al. (2014) catalog; (m) Brayley D, NAC frame M144836594L, 0.50 m/pixel, $i = 53.81°$; (n) Maclear-4, NAC frame M181030493L (also for panel o), 1.19 m/pixel, $i = 67.74°$; (o) Maclear-5; Maclear-4 and Maclear-5 IMPs are 1.1 km apart, and they lie between the #17 and #31 IMPs (28.7 km apart) in the Braden et al. (2014) catalog; (p) Maclear-6, NAC frame M1184689380R, 1.07 mm/pixel, $i = 68.18°$; this IMP is 1.7 km NW of the Arago-5 IMP in Braden et al. (2014) catalog, which are both on the flank of a small shield volcano; (q) Secchi X-1, NAC frame M119571034R (also for panel r), 0.48 m/pixel, $i = 57.24°$; (r) Secchi X-3; (s) Secchi X-4, NAC frame M1249261996R, 0.84-m/pixel size, $i = 65.63°$; this IMP is 6 km NW of #28 IMP in Braden et al. (2014) catalog; (t) Secchi X-5, NAC frame M121925686R, 0.48 m/pixel, $i = 29.77°$; this IMP is 1.5 km north of #62 IMP in Braden et al. (2014) catalog; (u) Vera, NAC frame M1173350317R, 1.27 m/pixel, $i = 71.29°$. All panels are sinusoidally projected with map center at the IMP identification site, and north is up (the same in Figures 7–12, 14, and 15).

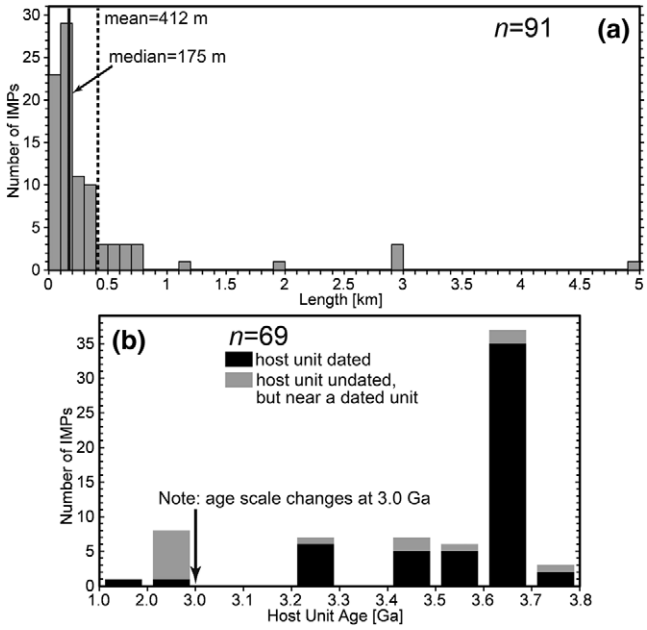


Figure 4. Histograms of (a) the maximum length of the 91 IMPs and (b) host mare unit age of 69 IMPs. The length-frequency of lunar IMPs (panel a) shows a leptokurtic distribution, with a positive skewness toward larger sizes, mean length of 412 m and median length value of 175 m. Note the horizontal axis (host mare age) scale of panel b changes at 3.0 Ga.

[~65%] dated global mare units; Figure 5). Only nine IMPs are located in two mare units emplaced later in the west nearside maria within the PKT terrain: (1) eight IMPs occurs in a very local region in SW Mare Imbrium and NW Mare Insularum (the Bessarion V IMPs and the Brayley D IMP), which are all located in or near the P43 mare unit (2.12 Ga; Hiesinger, van der Bogert, et al., 2011), and (2) another IMP (the Aristarchus North IMP; see more detailed characterization of this IMP in section 5 below) occurs in the P60 mare unit in Oceanus Procellarum (1.2 Ga; Hiesinger, van der Bogert, et al., 2011), adjacent to Aristarchus crater ejecta.

5. Geologic Settings and the Classification Scheme

We investigate the detailed geologic settings of each IMP occurrence using the latest image and altimetric data sets, including morphology, morphometry, topography, and geologic/tectonic setting, and propose a classification scheme of the geologic settings of the entire documented IMP population as follows (Figure 6 and Table 3):

5.1. Context #1: On the Floors of Small Shield Volcano Summit Pit Craters

We found four such IMPs, namely, Ina, Manilus-2, Cauchy-5, and #20 IMP in the Braden et al. (2014) catalog (Figures 7a– 7d) and a possible one (Maskelyne) (Figure 7f). Three of the IMPs in this category, Ina, Cauchy-5, and Maskelyne, are among the largest IMPs on the Moon, all with a maximum length of ~3 km, suggesting that lunar shield-building eruptions and summit pit crater activities may facilitate the development and emplacement of large IMPs (e.g., Qiao, Head, Ling, Wilson, Xiao, et al., 2019; Strain & El-Baz, 1980; Wilson & Head, 2017b). The other IMPs are much smaller, with a length between ~200 and ~350 m and are characterized by irregular shapes. The hosting shield volcanoes are observed to vary in size and topography. The Ina shield volcano is ~22 km in base diameter and ~320 m high (Figure 7a) and among the largest shield volcanoes on the Moon (Head & Gifford, 1980; Qiao, Head, Ling, Wilson, Xiao, et al., 2019). The Cauchy-5 small

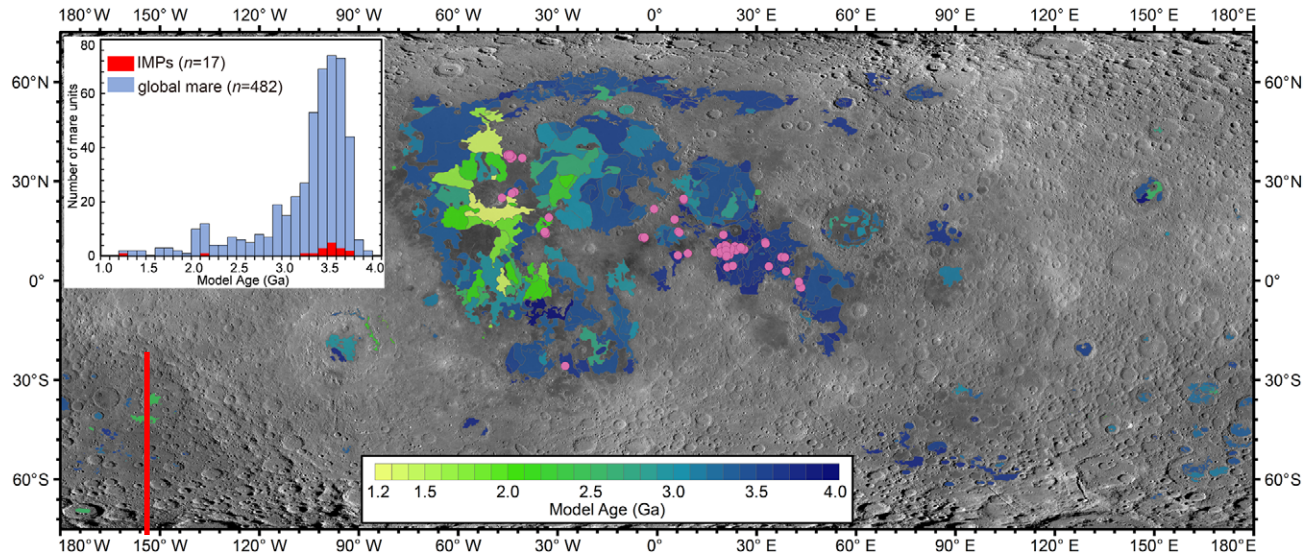


Figure 5. Distribution of the entire IMP population (pink dots) in the context of the global map of the model ages of mare basalts (color-coded). The insert panel shows the histogram of the temporal distribution of model ages of global lunar mare units (blue columns) and host mare unit ages of lunar IMPs (red columns). The model ages of global mare units (n = 482) are compiled from multiple previous investigations (Cho et al., 2012; Haruyama et al., 2009; Hiesinger et al., 2006, 2011, 2011; Morota et al., 2009, 2011; Pasckert et al., 2015, 2018; Tyrie, 1988; Whitten et al., 2011).

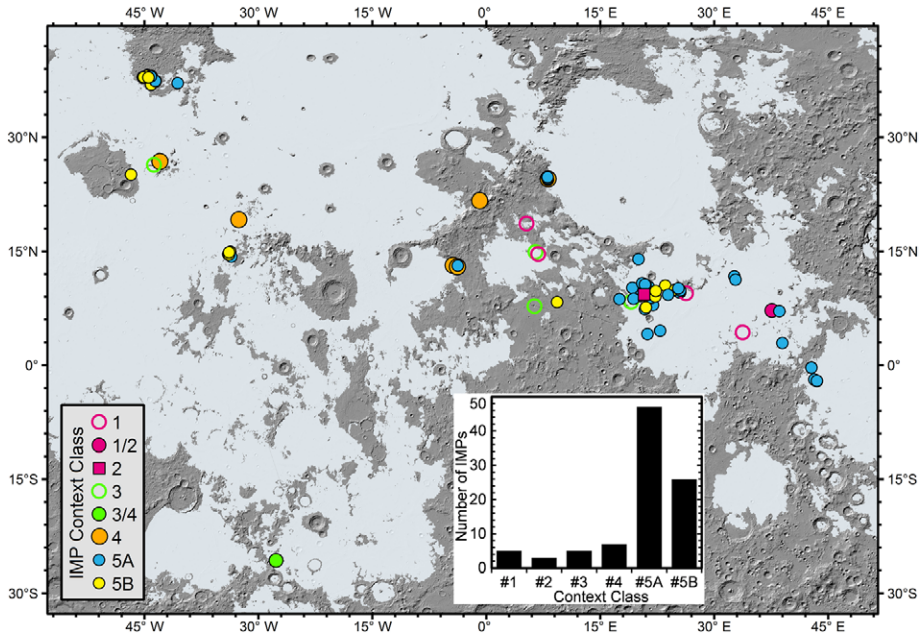


Figure 6. Spatial distribution of all identified IMPs in terms of the classification of their geologic context. The insert panel shows the histogram of IMP population in each context type.

shield volcano is ~5–6 km in base diameter and ~40 m high. It also displays an elongate summit pit crater, ~0.75 × 2.5 km and ~75 m deep (Figure 7b; Qiao, Head, Wilson, & Ling, 2018; Qiao et al., 2020). The Manilus-2 small shield was previously identified on telescopic photography and measured to be ~4.5 km in diameter (Head & Gifford, 1980); our updated measurement using Kaguya image and topography derives a ~5.0 × 5.5-km base diameter and a ~80-m shield height (Figure 7d). New high-resolution image data also resolve a summit pit crater which is ~0.7 × 0.5 km in diameter and ~30 m deep. The small shield volcano that hosts the #20 IMP is newly identified in this work. Kaguya TC DTM and SLDEM2015 topography show that it is a circular dome structure, ~6 × 5 km in base diameter and ~40 m high (Figure 7c). The flank of this shield is very gentle, with a kilometer-scale slope of <1°, explaining why it is not well resolved by image data and was not previously identified. The domical nature of the Maskelyne structure is suggested in low-sun angle images, with a base diameter of ~8.5 × 6.5 km, but is not well resolved on topography maps, as it is located on regional slopes and adjacent to several other domes (Figure 7f).

5.2. Context #2: On the Flanks of Small Shield Volcanoes

Three IMPs are identified in this category, namely, Cauchy-5 flank IMP (Figure 7b), Arago-5 IMP, and Maclear-6 IMP (Figure 7e). The Cauchy-5 small shield volcano hosts IMPs both on the summit pit crater floor (Context #1 IMP) and on the flank (Context #2 IMP) (Figure 7b). The Arago-5 (#9 IMP in the Braden et al., 2014 catalog) and Maclear-6 IMPs (newly identified IMP, Table 2) colocate on different portions of the Arago-5 small shield (Figure 7e). The Arago-5 shield has been previously identified on telescopic photographs and measured to be 8 km in base diameter (Head & Gifford, 1980). Updated Kaguya data-based morphometric and topographic investigation reveals the elliptical shape of this shield, oriented in a WNW direction, with a base diameter of ~7.7 × 5.1 km and ~90 m height above the surrounding mare (Figure 7e). The summit pit crater is developed at the eastern part of this shield, which is ~1.6 × 1.1 km in diameter and ~180 m lower than the pit rim, deeper than the mare surrounding the shield. IMP occurrences on the shield flanks are much smaller than those on the shield summit pit floor, with lengths less than 750 m.

5.3. Context #3: Within Linear/Sinuous Rilles or Pit Crater Chains

Five IMPs are identified in this category, namely, Sosigenes, Manilus-1, Hyginus IMP, Vera (newly identified; Table 2), and Nubium (Figure 8). Two of Context #3-type IMPs, Sosigenes and Nubium are among the largest IMPs on the Moon, with lengths of 5 and 2 km, respectively. The other three IMPs are much

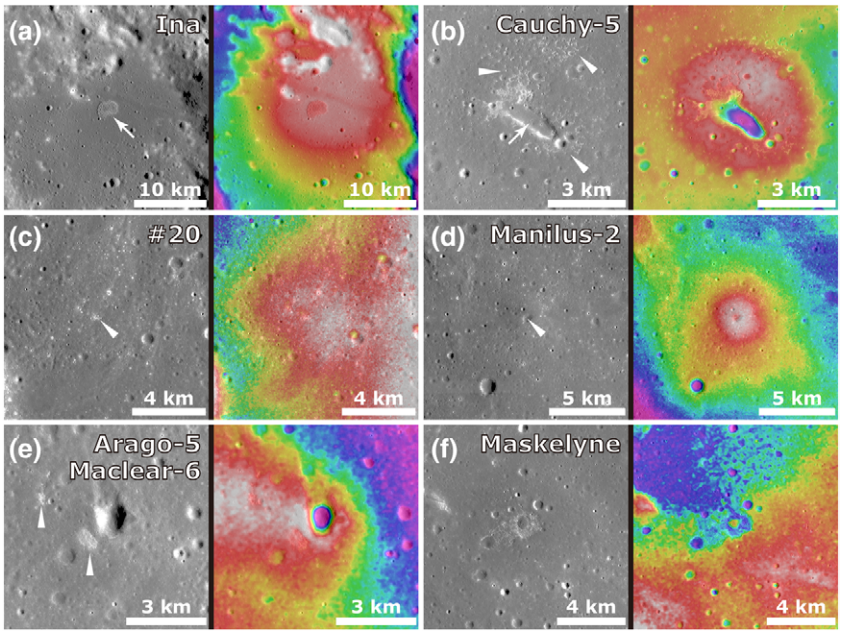


Figure 7. The geological context of lunar IMPs associated with small shield volcanoes: on the summit pit crater floor (Context #1; panels a–d) and on the flank (Context #2; panels b and e) and one possible Context #1 IMP (panel f). Each site is shown in an optical image (left column) and with a color topography map overlain (right column; red and white colors are higher elevations, and purple and magenta colors are lower elevations). (a) Ina, 18.65°N, 5.3°E, the arrow points to the IMP feature on the small shield pit crater floor, Kaguya TC evening map and SLDEM2015 topography. (b) Cauchy-5, 7.169°N, 37.592°E, the arrow points to the IMP occurrence on the small shield pit crater floor (Context #1 IMP) and the tips of elongated triangle mark the IMPs on the shield flank (Context #2 IMPs), LROC NAC M1108025067 and LROC NAC DTM. (c) #20 IMP, 9.432°N, 26.287°E, the tip of elongated triangle marks the IMP on shield summit pit crater floor, TC morning map and TC DTM topography. (d) Manilus-2, 14.628°N, 6.821°E, tip of elongated triangle marks the IMP on shield summit pit crater floor, TC morning map and TC DTM topography. (e) Arago-5 small shield, 9.259°N, 20.788°E, which hosts two IMPs on its flank: Arago-5 IMP (marked by the lower right elongated triangle) and Maclear-6 IMP (the upper left elongated triangle; Table 2), TC morning map and TC DTM topography. (f) Maskelyne, 4.33°N, 33.75°E, TC morning map and TC DTM topography.

smaller, with lengths between ~70 and ~270 m. The pit craters that host these IMPs are observed to vary in morphology and tectonic setting, while all are plausibly interpreted to be atop dikes (see Head & Wilson, 2017). The elongate Sosigenes pit, coaligned with a chain of pit craters, pit chains, and linear ridges, may represent the collapse of the gas cavity at the dike-tip (Qiao, Head, Xiao, et al., 2018). The Hyginus crater, ~10 km in diameter, occurs as a distinctive elbow in the ~215-km-long graben system and is interpreted to be formed by surface subsidence into an evacuated sill developed at the dike tip (Wilson et al., 2011). The Vera IMP (Table 2) occurs within the source depression of Rima Prinz, which has been interpreted to be the source depression of a sinuous rille-forming volcanic eruption site (Hurwitz et al., 2012). The Nubium IMP occurs on the floor of an elongate rille that is ~4.7 km long, up to ~1 km wide and ~80 m deep. The Manilus-1 IMP occurs on the floor of a depression that consists of two quasi-perpendicular rilles; the relatively larger rille, which also hosts larger IMPs, is ~1.2 × 0.7 km in size and up to ~55 m deep.

5.4. Context #4: On the Rim or in the Adjacent Exterior of Linear/Sinuous Rilles

Seven IMPs of this type are identified (Figure 9), namely, the Nubium IMP (arrow in Figure 8b), #21, #45, #50, #63 (in the Braden et al. (2014) catalog), Aratus D-5, and Brayley D (Table 2). Among these IMPs, four occur at the upper wall or rim of linear rilles (#21, #45, Aratus D-5, and Brayley D IMPs), and three occur in the adjacent exterior mare surface of linear rilles (Nubium, #50 and #63 IMPs), within a distance of up to ~1.7 km from the rille rim. These associated linear rilles are observed to vary in size and depth. The Nubium IMP rille is ~4.2 km long, up to ~1 km wide, and up to ~80 m deep (Figure 8b). The linear feature associated with #21 IMP is about 1.7 × 0.4 km in size and ~20 m deep (Figure 9a), the smallest rille associated

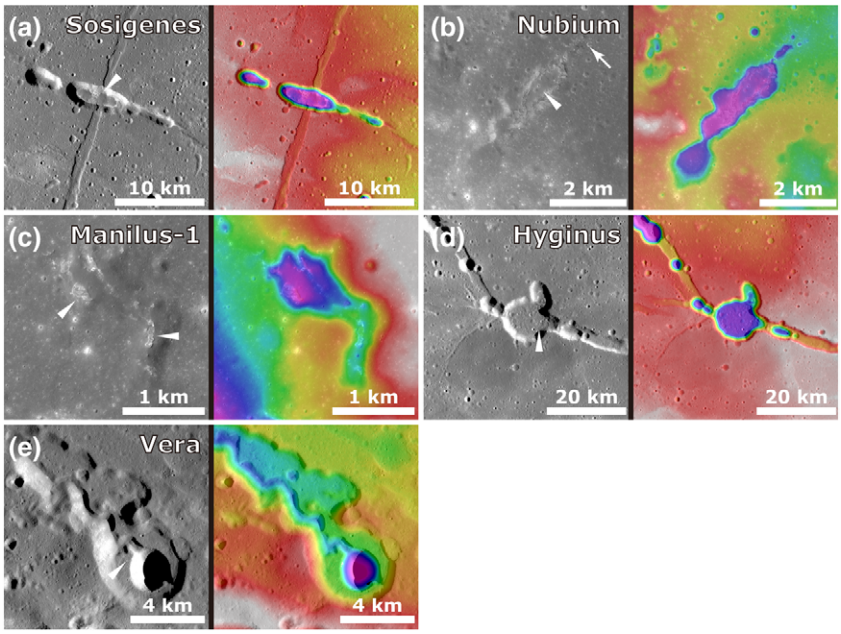


Figure 8. The geological context of lunar IMPs within linear/sinuous rilles or pit crater chains (Context #3 IMPs). Each site is shown in an optical image (left column) and with color topography map overlain (right column; red and white colors are higher elevations and purple and magenta colors are lower elevations). (a) Sosigenes, 8.335°N, 19.071°E, Kaguya TC evening map and TC DTM topography. (b) Nubium, 25.724°S, 27.681°W, LROC NAC M1167355858 and NAC DTM topography. (c) Manilus-1, 14.889°N, 6.467°E, NAC M1121188383 and NAC DTM topography. (d) Hyginus, 7.726°N, 6.35°E, TC morning map and TC DTM topography. (e) Vera, 26.342°N, 43.76°W, TC morning map and TC DTM topography. IMPs in pits are all marked by white elongated triangles, and the arrow in panel b points to an IMP occurrence outside the pit crater (a Context #4 IMP).

with IMPs in this category. The #45 and #50 IMPs are both associated with a huge linear rille in the east of Sinus Aestuum; the rille is ~90 km long, typically 1–1.3 km wide and ~170–270 m deep (Figures 9b and 9c). The #50 IMP is also in the adjacent exterior mare surface of an elongate pit crater, which is 6.9 × 3.4 km in size and up to ~860 m deep (Figure 9c). The sinuous rille associated with #63 IMP is one of the rilles of the Rimae Prinz and is 38 km long, typically 1–1.5 km wide and up to 165 m deep (#66 rille in the Hurwitz et al., (2013) list, Figure 9d). The associated rille of the Aratus D-5 IMP is ~6 km long, typical 0.4 km wide, and up to ~70 m deep (Figure 9e). The Brayley D IMPs is associated with an elongate pit ~5.6 km long, typically 1.5–1.8 km wide and up to ~450 m deep (Figure 9f). The spatial distribution map of Context #4 IMPs (Figure 6) indicates several ($n = 5$) of these IMPs appears to occur at the boundaries between maria and highlands. However, checking the local maps of these IMPs find they are still at a considerable distance from the mare boundary (ranging from ~5 to ~60 km), suggesting that basin-related tectonics and/or subsidence of mare basalts may not exert a dominant effect on the occurrence of lunar IMPs.

5.5. Context #5: IMPs in Typical Mare Deposits

These can be further divided into two subcategories:

5.5.1. Context #5A: In Relatively Flat Mare Plain

We have identified 47 IMPs in this subtype, making it the most common IMP type (Figure 10 and Table 3). The majority of Context #5A IMPs are associated with depressions within mare plains (mare pits) and are typically irregular and elongated in shape, similar to the many small pits observed on the Cauchy-5 shield flank (Figure 7b and Qiao, Head, Xiao, et al., 2018; Qiao et al., 2020). The geologic settings of these IMP types are diverse in characteristics and can be further classified into several subtypes. Some IMPs occur at the bottom of depressions in the mare plain (Figures 10a and 10i); these depressions are generally very shallow (generally less than ~5 m, measured from LROC NAC DTM topography; Figures 10c and 10l), while some of them seem to be relatively deep (generally greater than ~10 m and up to ~40 m, measured from

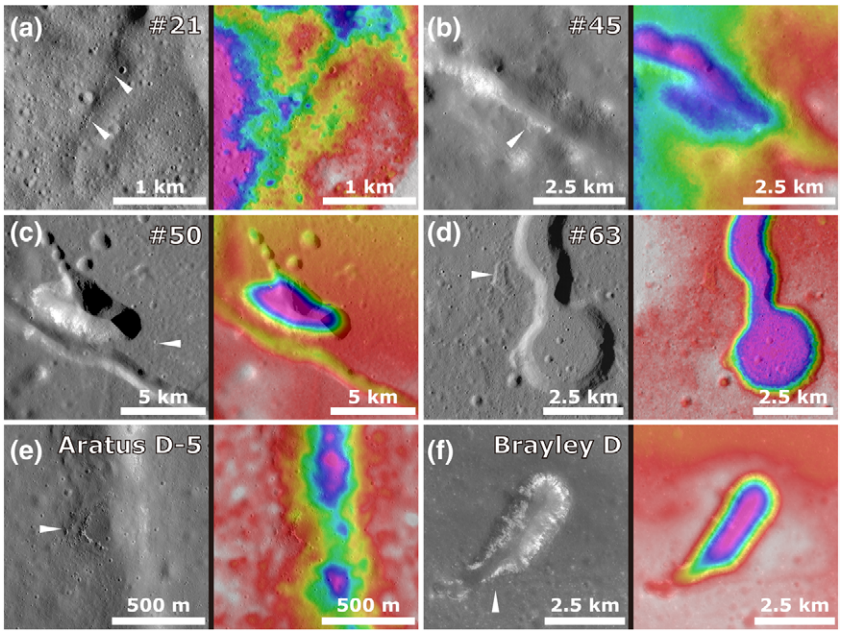


Figure 9. The geological context of lunar IMPs on the rim (panels a, b, e, and f) or in the adjacent exterior (panels c and d) of linear/sinuous rilles (Context #4 IMPs). Each site is shown in an optical image (left column) and with a color topography map overlain (right column; red and white colors are higher elevations and purple and magenta colors are lower elevations). (a) #21 IMP (in the Braden et al. (2014) catalog), 21.653°N, 0.865°W, LROC NAC M1203670820R and TC DTM topography (the rille is too small to be well resolved on the 10 m/pixel TC topography). (b) #45 IMP, 13.131°N, 4.361°W, NAC M1138937683L and TC DTM topography. (c) #50 IMP, 12.931°N, 3.806°W, TC morning map and TC DTM topography. (d) #63 IMP, 26.786°N, 42.959°W, NAC M1123882552L and TC DTM topography. (e) Aratus D-5 IMP (Table 2), 24.497°N, 8.130°E, NAC M150464022L and TC DTM topography. (f) Brayley D IMP (Table 2), 19.145°N, 32.579°W, NAC M1190926639 and NAC DTM topography. The IMPs are all marked by white elongated triangles.

Kaguya TC DTM topography; Figures 10e, 10g, and 10k). Some depressions are aligned in small pit chains (Figure 10d). These IMPs may occur at various locations in the associated depression. Some IMPs are present on the depression wall (Figures 10h and 10j), and some IMPs occur on both the depression floor and wall slopes (Figure 10f). Several IMPs occur in mare plains that infill the floors of impact craters (Figure 10b).

5.5.2. Context #5B: On Typical Mare Features and Structures

We identified 26 IMPs in this category (Figure 11 and Table 3). As with Context #5A, IMPs in this subtype are also located within mare regions, but they occur locally on topographically raised mare features/structures (Figures 11b, 11d, and 11i) or on the slopes of mare structures (Figure 3j). IMPs in this subtype generally share context characteristics with Context #5A IMPs in mare plains, though their geologic settings are relatively less diversified. In a manner similar to Context #5A IMPs, many IMPs in this type also occur at the bottom of depressions in mare deposits; these associated depressions are generally very shallow (generally less than ~5 m, measured from Kaguya TC DTM topography; Figure 11c). No deep depressions (greater than ~10 m), such as those associated with Context #5A IMPs, are observed in this subtype. Also similar to Context #5A IMPs, some IMPs in this category occur on the walls and rims of depressions (Figures 3h and 3i) and the exterior ejecta deposit of some impact craters (Figure 11e). In addition, several IMPs of this type are located on mare ridges (Figure 11f). Context #5B IMPs are generally very small (dominantly 100–200 m in length, Figure 11h), and only a few are larger (up to 1.2 km in length, Figure 11a).

One of the most enigmatic features among the entire IMP population is the one ~25 km north of Aristarchus crater (25.044°N, 46.767°W; termed North Aristarchus IMP in the Braden et al. (2014) catalog). It seems to be located on the continuous ejecta deposit of Aristarchus crater (Braden et al., 2014; Figure 12a), and it is also very close (~2.7 km) to the mare boundary mapped out by Nelson et al. (2014). Examination of high-resolution LROC NAC imagery (Figure 12c) and topography (Figure 12d) shows that the clusters of

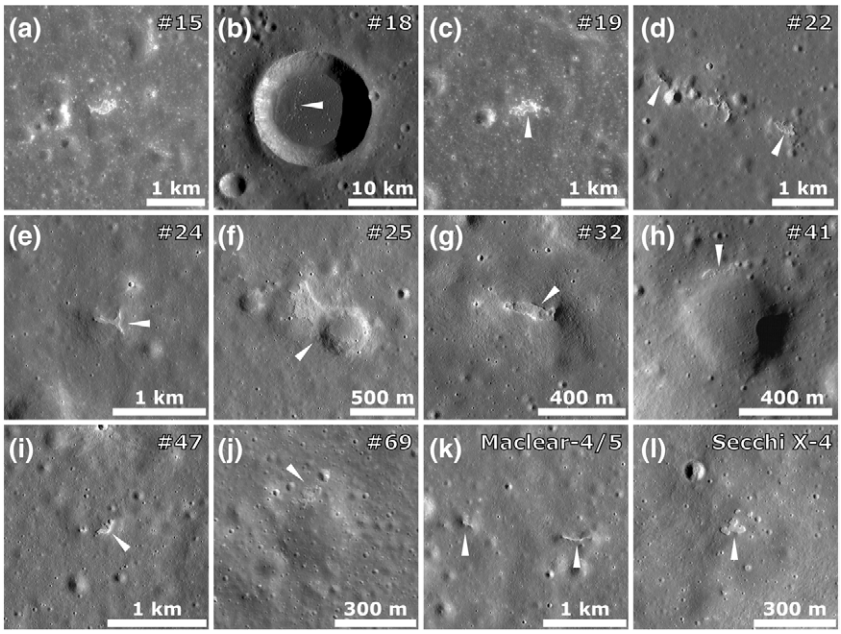


Figure 10. The geological context of representative IMPs in flat mare plains (Context #5A IMPs). (a) #15 IMP (in the Braden et al. (2014) catalog), 8.891°N, 21.487°E, LROC NAC M1175268761. (b) #18 IMP, 8.67°N, 17.51°E, Kaguya TC morning map. (c) #19 IMP, 9.564°N, 25.392°E, NAC M1190554377. (d) #22 IMP, 9.54°N, 20.22°E, NAC M162175239. (e) #24 IMP, 7.887°N, 21.937°E, NAC M181023296L. (f) #25 IMP, 11.235°N, 32.806°E, NAC M1157535724. (g) #32 IMP, 9.102°N, 20.265°E, NAC M162175239L. (h) #41 IMP, 37.304°N, 43.628°W, NAC M1154514667L. (i) #47 IMP, 7.083°N, 38.574°E, NAC M180916096R. (j) #69 IMP, 37.995°N, 44.159°W, NAC M1280383538R. (k) Maclear-4 IMP (left), 10.6°N, 20.94°E and Maclear-5 IMP (right), 10.604°N, 20.9°E, NAC M181030493L. (l) Secchi X-4 IMP, 1.882°S, 43.176°E, NAC M1249261996R. The IMPs are all marked by the white elongated triangles.

small IMPs forming this feature are actually located on local topographically high terrains, up to ~40–50 m higher than the surrounding surface. Iron abundance mapping results (using Kaguya Multiband Imager (MI) data and the Lemelin et al. (2015) algorithm) show that these topographic highs have a FeO content >14 wt.%, comparable with that of the adjacent mare (Figure 12b), indicating a basaltic composition for these terrains (either local mare basalts or distant mare materials ejected by the Aristarchus impact). On the basis of these observations, we suggest that the North Aristarchus IMP occurrences are located on mare features (possibly volcanic structures mantled with thin Aristarchus ejecta) and can be classified as a Context #5B IMP.

6. Characteristics and Classification

We next examine the detailed characteristics of all the 91 documented IMP features using high-resolution LROC NAC images, including structure, geomorphology, morphometry, and surface texture, and derive a classification scheme for IMP characteristics (Figures 13 and 14 and Table 3):

6.1. Characteristic Class #1: Composed of a Combination of Positive-Relief Mounds and Lower Rough Hummocky Terrains ("Mound + Floor" Type)

Five IMPs are identified in this category, namely, Sosigenes, Ina, Cauchy-5 (summit pit floor and rim), Maskelyne, and Nubium (#1–5 IMPs in the Braden et al. (2014) catalog; Figures 14a–14e). The five Class #1 IMPs are also the largest IMPs among the entire IMP population, with lengths ranging from 2 to 5 km, indicating that the building of the raised mounds requires a relatively high volume of lunar volcanic materials. The mounds are characterized by a bleb-like and convex meniscus appearance, and the lower hummocky units are characterized by ridged and pitted textures and often host block

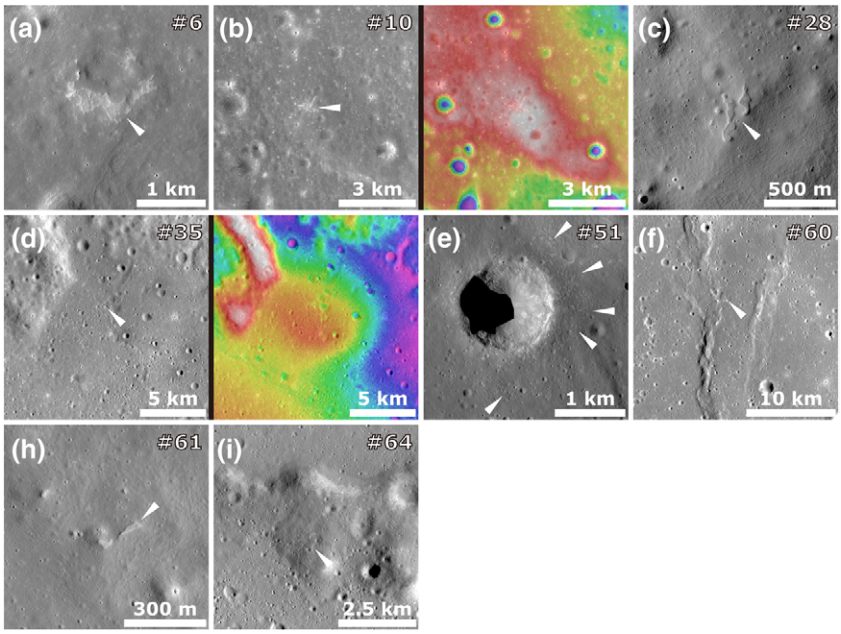


Figure 11. The geological context of representative IMPs in mare features and structures (Context #5B IMPs). Two sites (panels b and d) are shown in both optical image (left column) and with color topography map overlain (right column; red and white colors are higher elevations, and purple and magenta colors are lower elevations); the other sites are shown in optical images only. (a) #6 IMP (in the Braden et al. (2014) catalog), 10.46°N, 23.547°E, LROC NAC M1230568264R. (b) #10 IMP, 7.559°N, 20.984°E, NAC M1144665397 and NAC DTM topography. (c) #28 IMP, 38.152°N, 44.6°W, NAC M1154521777L. (d) #35 IMP, 8.279°N, 9.319°E, Kaguya TC morning map and TC DTM topography. (e) #51 IMP, 14.597°N, 33.979°W, NAC M1142674596. (f) #60 IMP, 9.012°N, 22.248°E, TC morning map. (h) #61 IMP, 9.738°N, 22.32°E, NAC M1096351025R. (i) #64 IMP, 14.468°N, 33.729°W, TC morning map. The IMPs are all marked by the white elongated triangles.

exposures (e.g., Braden et al., 2014; Garry et al., 2012; Qiao, Head, Ling, Wilson, Xiao, et al., 2019; Qiao, Head, Xiao, et al., 2018).

6.2. Characteristic Class #2: Composed of Rough, Bright Pit Terrains ("Pit Only" Type)

These IMPs host pit terrains resembling the floor terrains in Class #1 IMPs, while lacking the characteristic bleb-like raised mound structures. IMPs in this category are observed to occur in various locations and can be further divided into two sub-categories:

6.2.1. Characteristic Class #2A: Pit Only IMPs Within Mare Surface

We identify 65 IMPs in the category, making it the most common characteristic subclass of IMPs, including Cauchy-5 (shield flank, Figure 14c), Arago-5 (shield flank), Maskelyne (flank, Figure 14d), Maclear-2 IMP (Figure 14f), Aristarchus North IMP (Figure 14g), #22 IMP (Figure 14h), #35 IMP (Figure 14i), and Hyginus IMP (Figure 14k).

6.2.2. Characteristic Class #2B: Pit Only IMPs Associated With Depressions (at the Rim, Wall, or Floor) or on Slopes

47 IMPs occurrences are classified into this subtype, including Cauchy-5 flank (Figure 14c), Maskelyne (flank, Figure 14d), Aristarchus North IMP (Figure 14g), #35 IMP (Figure 14i), Manilus-2 (summit pit, Figure 14j), Hyginus IMP (Figure 14k), and #58 IMP (Figure 14l). The depressions associated with Class #2B IMPs show variable characteristics and origins. Many are characterized by a circular map view, bowl-shaped profile, and raised rim crest (Figures 14c and 14l), revealing that these depressions are typical small impact craters. Some associated depressions are characterized by irregular shapes and cross-sectional profiles (e.g., Figures 3h, 14g, 14i, and 14l), which probably represent collapse depressions of several types, like drainage pits. At two IMP occurrences, the associated depressions are probably endogenetic in origin: the Manilus-2 IMP depression occurs as a summit pit of a small shield volcano (Figures 7d and 14j), and the #45 IMP occurs on the interior wall and rim of a long linear rille (Figure 9b). Various subtypes of

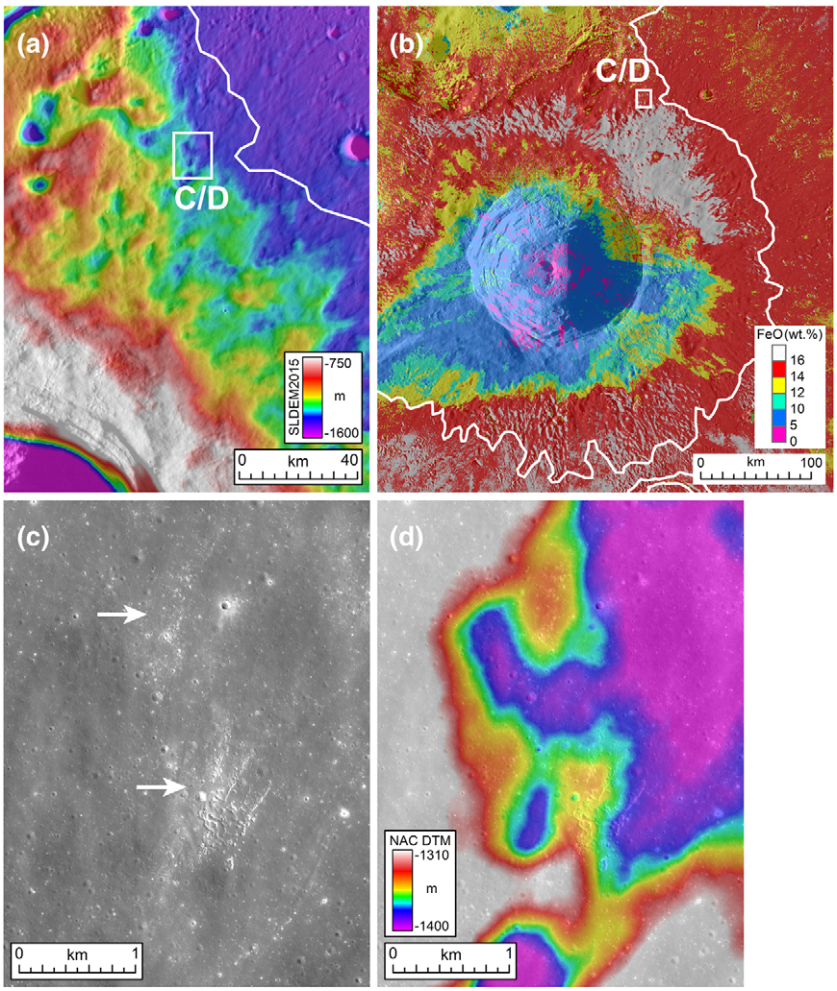


Figure 12. Geological context of Aristarchus north IMP (25.044°N, 46.767°W): (a) SLDEM2015 topography overlain on LROC WAC low-sun image, (b) FeO abundance map calculated from Kaguya multiband imager (MI) data using the Lemelin et al. (2015) algorithm, (c) LROC NAC frame M1114476549, and (d) NAC DTM topography overlain NAC M1114476549. The white rectangles in panels a and b mark the extent of panel C/D, the white polygons in panels a and b are the mare boundary mapped by Nelson et al. (2014) and the white arrows in panel c point to the two clusters of small IMPs.

associated depressions are also accompanied by characteristic spatial distribution patterns of the IMP occurrences. In the impact crater case, the IMPs are often around the upper inner wall, hinting at their formation below the surface of the preimpact mare and revealing a layer of unusual properties (probably highly vesicular basalt; Wilson & Head, 2017b; Qiao, Head, Ling, Wilson, Xiao, et al., 2019) exposed by the impact. In the collapse depression case, it is possible that a large collapse depression formed over an area of magmatic gas voids or possibly a buried crater, where the formation of gas might have been enhanced by the locally thicker lava.

6.3. Surface Textures of the Floor Terrains of Lunar IMPs

The various types of IMP occurrences share a lot of similarities but also show many differences: both the lower hummocky units of Class #1 IMPs and pit terrains of Class #2 IMPs are characterized by complicated surface textures, including blocky, ridged, and vermicular terrains, but the Class #2 IMPs lack the characteristic mound terrains observed at Class #1 IMPs. We use our prior detailed characterization of Ina floor terrain surface textures as a frame of reference (Qiao, Head, Ling, Wilson, Xiao, et al., 2019: section 3.5 and

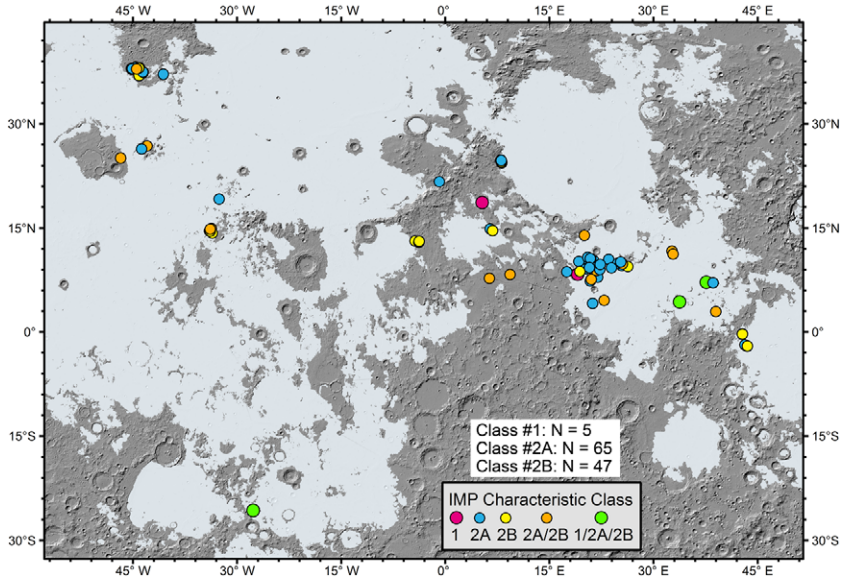


Figure 13. Spatial distribution of all identified IMPs in terms of the classification of their characteristics and structure.

Figure 13) and survey the detailed textures of other IMP occurrences (floor hummocky terrains of Class #1 IMPs and pit terrains of Class #2 IMPs; Table 3). Surface textures of Ina floor terrains include (1) relatively smooth texture, (2) hummocky texture, (3) pitted texture, (4) ridged texture, (5) polygonal texture, (6) vermicular texture, and (7) blocky texture (Figures 15a and 15b). Additional texture subtypes observed at other IMP occurrences are (8) uneven texture and (9) bright streak (Figure 15c): uneven textures are characterized by rough and coarse morphology, while lacking the small domical structures of the hummocky textures; and bright streaks are characterized by elongations downslope, relatively higher albedo than their surroundings and no detectable topographic relief. Various types of floor terrain textures often co-occur at one single IMP (Table 3). The statistic histogram of texture type occurrence shows that the hummocky, pitted, blocky, and uneven textures are the most common types of textures, which are present (either occur alone or co-occur) at almost all IMPs (Figure 15d).

We also employ the LROC NAC DTM topography-derived slope maps to characterize the topographic slope of the various surface textures of the IMP floor terrains (Figure 15e). We find that the slopes of the various texture types do not correspond exactly to their morphological patterns, as the same type of texture may have a range of topographic slopes and various kinds of textures may have comparable slopes. We attribute this disparity to the contrasting resolution/baseline of the source data from which the morphology and topographic slope are interpreted: the morphology is derived from LROC NAC images with a typical pixel size of ~0.5 m, and the topographic slope map is calculated at a baseline of 6 m (2-m/pixel NAC DTM) or 15 m (5-m/pixel NAC DTM); the dimension of many textures of IMP floor terrains (for instance, hummocky, and pitted features) are, however, just between the LROC NAC pixel size and slope map baseline, making them observable on NAC images but unidentifiable on slope maps. However, comparison of the slope measurements still shows apparent differences between the various surface texture patterns. Smooth and uneven textures are characterized by the smallest slopes (though with a relatively wide slope range due to the aforesaid baseline effect); this is evidenced by their observed relatively simple texture and relief. Hummocky, pitted, ridged, and polygonal texture types are observed to all have comparable slopes to those of the smooth textures (~3–6°), though they have much more complicated and differentiated surface textures than the latter from NAC images, which can be explained by the fact that most of these texture units are shorter than the slope baseline. The vermicular textures are characterized by a slightly elevated slope (~6.5°), which is attributed to the observed much larger size of these vermicular structures (larger than the ridged units and slope baseline). The blocky textures have even steeper slopes (typically ~10°); this is consistent with their observed rugged appearance, topography and position (often in the topographical moats surrounding the mound

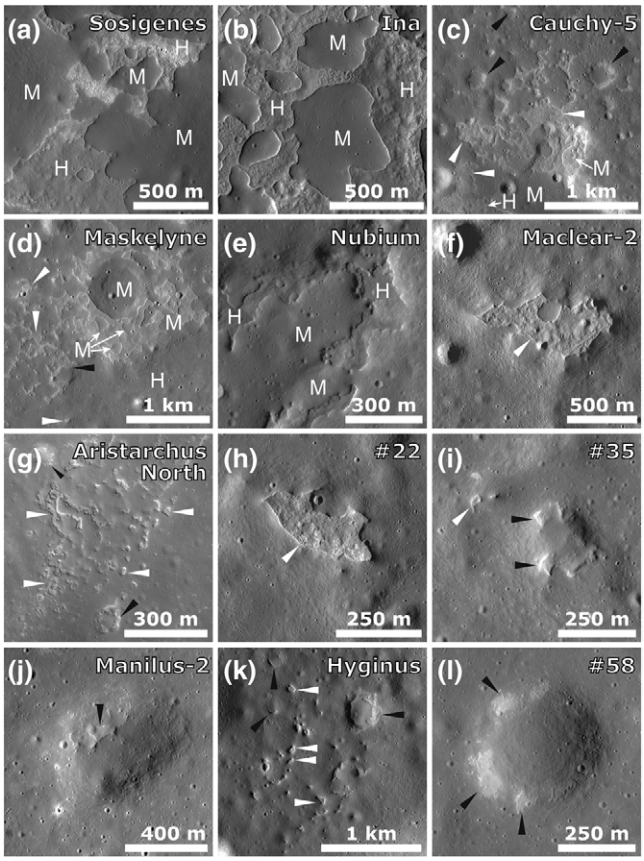


Figure 14. Detailed characteristics of representative IMPs in each type: being composed of a combination of mounds and lower rough hummocky terrains (Class #1, panels a–e) and being composed of rough, bright pit terrains within mare surface (Class #2A, panels c, d, f–i, and k) and associated with depressions (Class #2B, panels c, d, g, i, j–l). (a) Sosigenes, 8.335°N, 19.071°E, LROC NAC M192824968. (b) Ina, 18.65°N, 5.3°E, NAC M1138873574. (c) Cauchy-5, 7.169°N, 37.592°E, NAC M1218710334L. (d) Maskelyne, 4.33°N, 33.75°E, NAC M1215204344. (e) Nubium, 25.724°S, 27.681°W, NAC M1142616950L. (f) Maclear-2, 9.102°N, 20.298°E, NAC M1276451476R. (g) Aristarchus north IMP, 25.044°N, 46.767°W, NAC 168509312R. (h) #22 IMP, 9.54°N, 20.22°E, NAC M162175239L. (i) #35 IMP, 8.279°N, 9.319°E, NAC M1123533772L. (j) Manilus-2, 14.628°N, 6.821°E, NAC M192910855R. (k) Hyginus IMP, 7.726°N, 6.35°E, NAC M1157706629. (l) #58 IMP, 2.008°S, 43.333°E, NAC M1230441915R. The mounds and hummocky terrains of Class #1 IMPs are marked with "M" and "H", respectively. Class #2A and Class #2B IMPs are marked with the white and black elongated triangles, respectively. The rough terrains are observed to have various surface textures and the most common texture types are, in descending order, blocky, uneven, hummocky, and pitted floor textures.

terrains). The bright streak textures are characterized by the steepest slope (typically >10°) among all the observed floor terrain texture types, as they mainly occur on the slopes of volcanic structures.

7. Discussion

7.1. Association Between the Sizes, Geologic Contexts, and Characteristics of Lunar IMPs

The IMP populations in various geologic context and characteristic categories are observed to have quite different dimensions (Figures 16a and 16b). One of the main observations is the distinctly larger size of lunar IMPs in Contexts #1 (within shield summit pits, median length of 2.5 km, and maximum length of 3 km) and #3 (within other endogenetic pits, median length of 270 m, and maximum length of 5 km) than other IMPs (Figure 16a), indicating that the geologic settings of being contained within a pit crater may be the key factor for the development and emplacement of large IMPs. However, several IMPs in these two context categories are also relatively smaller (70–350 m in length), showing that being contained within a depression does not ensure the development of large IMPs and additional factors are involved. In these two characteristic classes of lunar IMPs, Class #1 IMPs (mounds + floor type, median length of 2.6 km, and maximum length of 5 km) are just the top five largest IMPs among the entire IMP catalog and are overwhelmingly larger than IMPs in any other category (pit only type; Figure 16b), suggesting the requirement of large volumes of building materials for the development of the raised mounded terrains.

The entire IMP population also shows subtle associations between the classification scheme in terms of the geologic context and the characteristics (Figure 16c). The special Class #1 IMPs with distinctive mound terrains (mound + floor type) exclusively occur within volcanic pit craters (Contexts #1 and #3), illustrating a close link between the geologic context (being contained within a pit crater) and the evolution of lunar IMP-formation process (emplacement of uplifted mound terrains). These IMPs are also among the largest and best-studied IMPs (e.g., Braden et al., 2014; Garry et al., 2012; Qiao et al., 2017, 2020; Qiao, Head, Ling, Wilson, Xiao, et al., 2019; Qiao, Head, Xiao, et al., 2018; Schultz et al., 2006; Strain & El-Baz, 1980). The pit only type IMPs (Class #2) mostly occur on mare regions (Contexts #5A and #5B), suggesting another important association between mare context and the origin of small IMP occurrences. In addition, the two IMP clusters, mound + floor type and pit only type, co-occur at three IMP features (Cauchy-5, Maskelyne, and Nubium), some of which show clear geologic setting links between the two IMP populations (especially the IMPs at the Cauchy-5 summit pit and flank, Qiao, Head, Xiao, Wilson, & Ling, 2018; Qiao et al., 2020), showing a promising potential for relating the origin of the two IMP populations.

7.2. Implications of the Classification Scheme Results for Models of Origin of Lunar IMPs

Although specific detailed studies are needed for each of the individual occurrences of IMPs, the updated classification scheme and the insights provided by subclassification guided by geologic context and IMP internal characteristics provide new insights and directions for future research. Specifically, of the six hypotheses previously proposed for the origin of lunar IMPs (Table 1), the diversity of environments, settings, and characteristics outlined here suggests that single process models, such as sublimation (Whitaker, 1972), pyroclastic eruptions (Carter et al., 2013), and removal of surface regolith by episodic

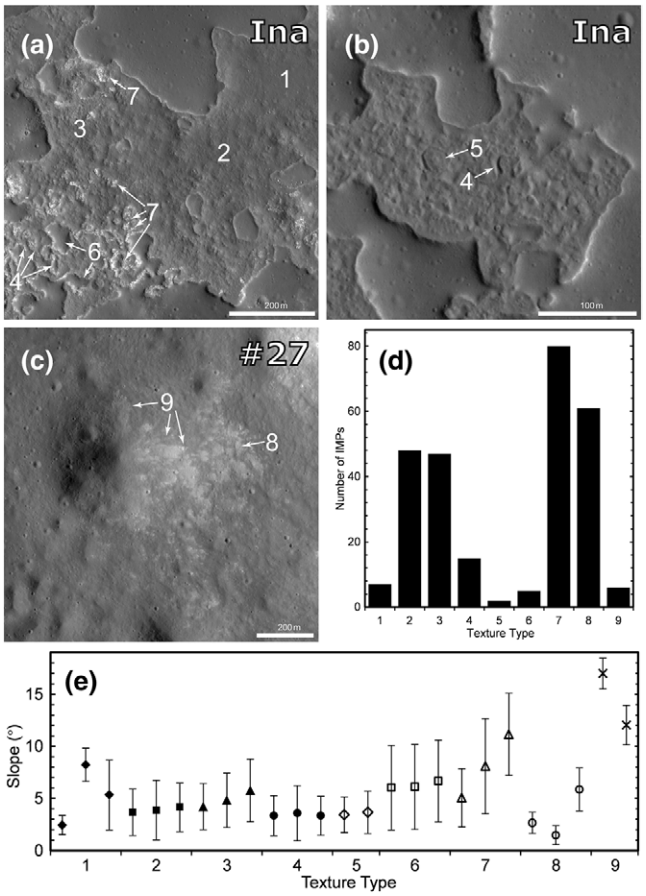


Figure 15. Various types of surface textures of the floor terrains of lunar IMPs presented at (a) the southeastern margin of Ina floor (centered at 18.642°N, 5.331°E), LROC NAC M119815703 (also for panel b), (b) the central floor of Ina (centered at 18.668°N, 5.303°E), and (c) #27 IMP, NAC M1173279016L. The surface texture types are marked with numbers: (1) smooth terrain, (2) hummocky, (3) pitted, (4) ridged, (5) polygonal, (6) vermicular, (7) blocky, (8) uneven, and (9) bright streak. (d) The histogram of IMP population having each texture type. (e) The LROC NAC DTM-slope (mean value $\pm 1\sigma$) of the various surface texture types at representative lunar IMPs: #1–7 texture types are of the Ina floor terrain, #8 texture type is of Cauchy-5 shield flank pits, and #9 texture type is of #64 and Bessarion-V-3 IMPs.

out-gassing within the past 10 Ma (Schultz et al., 2006), are insufficient to account for the wide range of observations. Instead, more complex processes, involving several stages and geologic processes, appear to be more likely. For example, the geologic context of occurrences associated with volcanic vents (e.g., floors of pit craters on the summits of small shield volcanoes; interior of sinuous rille source depressions) and volcanic constructs (the rim and flanks of small shield volcanoes; the rim of sinuous rille source depressions) both point to volcanic processes operating in the source region.

Their preservation in the relatively youngest deposits in the specific occurrences also favors modes of origin that operate in the later stages of the evolution of vents and associated eruptions. Thus, new developments in understanding the sequence of stages in lunar mare basalt eruptions (e.g., Wilson & Head, 2018) may provide insights into a wider range of temporal behavior (particularly volatile release patterns) in observed lunar volcanic eruptions and the IMPs. For example, the association with final-stage activity in closely related vent areas such as shield volcano summit pit craters would seem to favor proposed origins such as small lava intrusions within a collapse caldera atop an extrusive volcanic dome (e.g., El-Baz, 1972, 1973; Strain & El-Baz, 1980), lava flow inflation (e.g., Garry et al., 2012), or lava lake processes and magmatic foam extrusion (e.g., Qiao et al., 2017; Qiao, Head, Ling, Wilson, Xiao, et al., 2019; Qiao, Head, Xiao, et al., 2018; Wilson & Head, 2017b).

In addition, the close association of these IMP contexts with ancient volcanic edifices (>3 Ga) raises the question of why the CSFD ages of the major IMPs point to ages of <0.1 Ga (Braden et al., 2014) and suggest that alternate explanations should be investigated to account for the apparently abnormally young CSFD ages that occur in close geologic association with features formed over 3 Ga earlier.

Finally, the geologic context of small IMPs as isolated occurrences associated with ancient lunar mare deposits, initially reported by Braden et al. (2014) and reiterated here with our larger IMP population, provides new insights into IMP origins and directions for further research. The classification reported here underlines the characteristics of these small IMP occurrences and shows that they are dominated by deposits analogous to the rough floor unit in the larger occurrences, with only minor occurrences of the distinctive mound units seen in the larger examples. This suggests that the optical immaturity of the small IMP occurrences may be related to drainage into subsurface voids, a process that could occur due to subsequent superposed impact craters over billions of years following the initial emplacement of the flows. Such voids might be related to the latter stages of lava flow emplacement several billion years ago in which flow inflation and second boiling might occur, creating subsurface void spaces and macrovesicular substrates (e.g., Wilson & Head, 2017b, 2018) susceptible to subsequent collapse due to superposed impacts.

On the basis of (1) our previous theoretical treatment and observational investigation of the formation mechanism of several representative lunar IMPs (including Ina, Sosigenes, and Cauchy-5; Wilson & Head, 2017b; Qiao et al., 2017, 2020; Qiao, Head, Xiao, et al., 2018; Qiao, Head, Ling, Wilson, Xiao, et al., 2019) and (2) the new classification scheme presented here, we address that the described waning-stage magmatic foam formation and extrusion scenario is also applicable to the origin of lunar IMPs of various classes catalogued in this study and the wide range of observed characteristics can be largely explained in this eruptive context.

Guided by the documented features at representative lunar IMPs, especially Ina and Cauchy-5 (Qiao et al., 2020; Qiao, Head, Ling, Wilson, Xiao, et al., 2019), we find that the various geologic contexts of

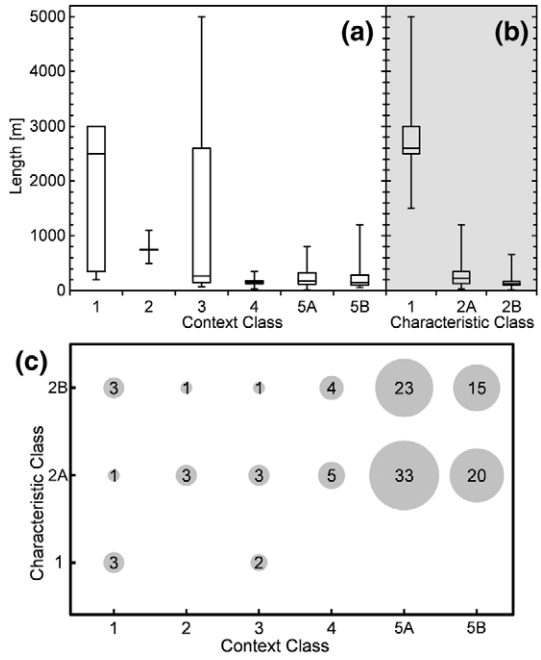


Figure 16. The minimum, first quartile, median, third quartile and maximum length of the entire IMP population in each (a) context and (b) characteristic class, and (c) the occurrence frequency (proportional to the bubble size) of lunar IMPs in terms of their context (horizontal axis) and characteristic classes (vertical axis).

lunar IMPs (Contexts #1–5 in section 5) can be generally grouped into two major categories: (1) pit crater environment (Contexts #1 and #3; being contained within a pit crater, or closed environment) and (2) (near-vent) mare flow environment (Contexts #2, #4, and #5; not being contained with a pit crater, simply emplaced on maria, or open environment).

In the pit crater environment, upwelling magma in the waning stages of the eruption would accumulate within the pit crater and formed a lava pond. Decrease of the magma ascent rate to less than ~1 m/s favored gas bubble (mainly CO) production and coalescence, initiating a Strombolian activity phase. This phase would deform, disrupt, and fracture the cooling lava lake crust; a solidified lava lake crust characterized by abundance vesicularity and macroporosity would be the resultant deposits (the lower rough and hummocky terrains of Class #1 IMPs). In the final stage of the eruption, the magma rise rate had become negligible and no additional magma would ascent from depth, H_2O gas exsolution produced viscous magmatic foam with an extreme vesicularity up to ~95% below the chilled lake crust. The final-stage dike closure caused the foamy magma extruded out onto the rough pit crater floor crust to produce the bleb-like raised mounds (the mound terrains of Class #1 IMPs). This formation scenario is consistent with our observations that all Class #1 IMPs are located in pit crater environments (Contexts #1 and #3, Figure 16b). Only in this context of being contained within a pit crater, the extruded magmatic foams can be potentially thick enough to build up the large (much larger than IMPs of other categories; Figure 16a) and raised mound terrains. However, being contained within a pit crater does not assure the development of raised mounds, as the extruded waning-stage magma foam can be simply not voluminous enough to do that, consistent with the occurrences of several Class #2 pit only IMPs in pit crater environments (Figure 16b).

In the (near-vent) mare flow environment, instead of being contained by a summit pit crater or collapse crater and forming a lava lake, the final-stage, very vesicular, and foamy magma would exit the fissure vent and overflow onto the adjacent surface beyond the vent rim (including shield flanks (Context #2) and the exterior of volcanic rilles (Context #4)) or spread out across the maria (Context #5) as a cooling and meter-thick foamy lava flows (Qiao et al., 2020). Subsequent meteoritic impacts into the emplaced foamy flows caused collapse of voids of various scales and shapes. Collapse in the foamy lavas was likely to expose the fresh and more coherent interior of the void-rich flows at the depression floor and/or upper walls, consistent with the observed bright and rough textures of the pit terrains of Class #2 IMPs (section 6 and Figure 14). The high porosity and inhomogeneous substrate properties of the foamy flows resulted in the postemplacement crater formation and impact-derived collapse process to be very atypical and complicated, generating the irregular crater appearance and various surface textures of the floor terrains of lunar IMPs (hummocky, pitted, blocky, uneven, etc.; section 6.3 and Figure 15). Some of the extruded foamy lava might flow and emplace on topographically raised terrains (including mare structures and mare ridges for Context #5B IMPs) or sloped surface; impact-derived collapse of these flows would potentially result in the observed "bright streak" surface texture patterns at the pit terrains of several small Class #2 IMPs (section 6.3).

7.3. Outstanding Unanswered Questions

The origin of lunar IMPs is one of most debated topics of lunar volcanism and geological evolution history. The formation age, emplacement mechanism, evolution during the formation process, properties of the resultant deposits, and postemplacement modification and its effect on the current observations represent key parts of any IMP origin model. The different and competing theories for their origin have already raised a list of outstanding questions about lunar IMPs (Table 1). Our new classification scheme in terms of the geologic settings and characteristics of lunar IMPs has contributed to address some of these key questions concerning the origin of lunar IMPs (section 7.2), but it also specifically introduces a second set of outstanding questions that adds to and complements the first set of questions, each meriting further investigations:

1. Why are lunar IMPs so uncommon in the lunar maria? The vast majority of lunar IMPs, especially smaller pit-type IMPs (Class #2), are found in lunar maria. But only a very small percent of stratigraphically defined mare units (17/482 = 3.5%, section 4) host lunar IMPs and no IMPs have been identified on lunar farside maria. If low effusion rates and foam buildup are typical of each mare volcanic eruption (e.g., Wilson & Head, 2017a, 2018), then why do not we see lunar IMPs everywhere? It is possible that even the most common mare deposit-forming eruptions may also operate in very different phases and styles and lead to widely varying resultant deposits, modulated by a range of factors including effusion rates, eruption durations, cooling and supply limitations to flow length, and preexisting topography (Head & Wilson, 2017). Our recent theoretical treatments of lunar basaltic volcanic eruptions suggested that gas release patterns and vesiculation processes are especially crucial in determining the final resultant disparate volcanic deposits including lunar IMPs (Wilson & Head, 2018). Lunar IMPs hosting maria are probably formed by volcanic eruptions defined by a narrow parameter space. Theoretical and observational analyses of mare volcanism and the final-stage volatile exsolution physics will provide an important framework for revealing the formation environment and evolution of lunar IMPs.
2. Why are IMPs so uncommon in small lunar shield volcano pit crater floors? Lunar small shield volcano summit pit floors are one of the common geologic settings of IMPs and host some of the most prominent examples, including Ina and Cauchy-5. Small shield volcanoes are common on the Moon. Over 300 small shields have been identified and dozens of them developed summit pit craters (e.g., Head & Gifford, 1980; Tye & Head, 2013). However, only five small shield pit crater floors host IMP features (Figure 7). These observations raise a line of questions concerning lunar shield-building eruptions, summit pit activities and the resultant deposits. What are the detailed morphologies of all small shield volcano pits and their variations? What do their flanks look like? What are the roles and effects of the total volume of involved magma and the behavior of waning-stage pit crater processes (a combination of extrusion of foams from below the lava crust, drain back, cooling and thermal contraction, monotonic or punctuated decline in the final effusion rates, etc.)? Each of these questions deserves further analyses. A general survey of global lunar small shield volcanoes has not been conducted since the preliminary analyses in 1980 that employed nearly half-century-old imagery sets (Lunar Orbiter, Apollo, etc.), which already showed that lunar small shields varied widely in geologic settings, association with other features, outlines, base diameters, cross-sectional shapes, and summit craters (presence or absence, dimension). These initial observations indicate contrasting processes in their formation and evolution (Head & Gifford, 1980), and it is possible that the IMP-related shield volcanoes are formed under very particular eruption conditions. In addition, the detailed topography, morphology, and texture of the summit pit and flank have yet to be examined in details due to the lack of images and topography data of sufficient resolution in prior investigations. The newly acquired submeter-scale LROC NAC images and high-precision LOLA altimetric measurements will provide an unprecedented opportunity for such investigations. Moreover, a detailed compositional analysis of the entire population of lunar IMPs and small shield volcanoes could also help answer this outstanding question.
3. What are the implications of these associations and characteristics for the debate about the age of IMPs? The emplacement age of lunar IMPs is one of the most debated topics of lunar geosciences (e.g., Stopar et al., 2019). Prevailing ideas include outgassing removal of surface regolith within the past 10 Ma (Schultz et al., 2006), geologically very recent (within the past 100 Ma), small volcanic eruptions (Braden et al., 2014), and ancient (>3 Ga) volcanism producing highly vesicular deposits (Qiao, Head, Ling, Wilson, Xiao, et al., 2019). We suggest that the age of the host mare units (Figures 4b and 5) and the geologic settings (Figure 6) can provide instructive information on determining the formation and age of lunar IMPs: interpretation for the formation mechanism and age of the IMPs must incorporate the facts that the vast majority of lunar IMPs are located in ancient mare volcanic deposits. Determining the age of lunar IMPs will provide direct key constraints on the cessation time of lunar volcanism (<100 Ma or ~1 Ga?) and strengthen our knowledge of lunar geologic and thermal evolution history, including the current thermal status of the lunar interior, the inventory of lunar heat-producing elements, and the global stress state field of the lunar lithosphere.
4. How is our understanding of lunar IMPs limited by the current observations and what new measurements from future exploration missions would unambiguously answer these questions? We address that the current limitations on the nature and origin of lunar IMPs include the quantitative physical properties, microstructures (e.g., small fractures) and porosity of IMP deposits (mound and floor terrains),

shallow subsurface structure and properties, and the detailed impact cratering mechanism in highly porous targets and the resultant effects on crater retention age estimations. Needed new measurements from future exploration endeavors include (a) orbital missions: dedicated high-resolution photometric and/or polarimetric measurements to constrain the microstructure (including subresolution roughness and particle sizes) of the surface of lunar IMPs, for instance, the Wide-Angle Polarimetry Camera (PolCam) to fly on the forthcoming Korea Pathfinder Lunar Orbiter (Sim et al., 2019); (b) landed missions: cameras, microscopic imagers, seismometers, penetrometers, and other geophysical instruments to determine the surface and shallow subsurface physical properties and structures (e.g., the Irregular Mare Patch Exploration Lander (IMPEL) mission concept; Draper et al., 2018), and in situ radiometric dating measurements to determine the crystallization age of IMP deposits, for example, the Chemistry, Organics, and Dating EXperiment (CODEX) mission concept (Anderson et al., 2017); (c) sample return missions: providing direct and high-precision radiometric dates, petrography, chemical, and isotopic compositions for the deposits of lunar IMPs, readily distinguishing their crystallization age and deposition mechanism. In addition, laboratory and numerical simulation experiments on the detailed impact cratering mechanism in highly porous targets and the resultant effects on crater retention ages would also contribute to uncover the formation age and postemplacement evolutions of lunar IMPs.

8. Conclusions

We compiled all previous lunar IMP identifications since the Apollo era and present an updated, comprehensive inventory of 91 lunar IMPs, which expands the known IMP occurrences into two additional nearside maria: Mare Serenitatis and Mare Imbrium. The ages of the maria hosting lunar IMPs are documented and show that the majority occur in mare units emplaced more than three billion years ago, contemporaneous with the climax of global lunar volcanism, suggesting that alternate formation mechanisms of lunar IMPs should be investigated in reference to their apparently abnormally young CSFD ages. We then surveyed the detailed geological characteristics of each IMP feature using the latest high-resolution image and altimetric data sets and derived classification schemes for all catalogued IMPs in terms of their geologic settings and characteristics. The entire lunar IMP population is observed to occur in a range of geologic settings, which are categorized into small shield volcano summit pit floor (Context #1) and flank (Context #2), pit crater chain or linear/sinuous rille interior (Context #3) and adjacent exterior (Context #4) and typical mare deposits (Context #5A: mare plain and Context #5B: mare volcanic edifices). The characteristics and structure of IMPs themselves were classified into mound + floor type (Class #1) and "pit only" type (Class #2A: within maria and Class #2B: associated with depressions). Our updated catalog and new classification scheme of lunar IMPs showed that the wide range of geologic settings and characteristics was consistent with the waning-stage magmatic foam formation and extrusion scenario in different environments: (1) in the pit crater environment (Contexts #1 and #3), waning-stage lava lake magmatic foam extrusions within the pit crater produced magmatic foam deposits (the mound terrains of Class #1 IMPs) superposed on the chilled lava lake crust (the lower hummocky terrains of Class #1 IMPs); (2) in the (near-vent) mare flow environment (Contexts #2, #4, and #5), impacts into the overflowed thin foamy flows across the maria resulted in void collapse, exposing the fresh and coherent interior of the solidified magma foams (rough and bright pit terrains of Class #2 IMPs). In addition, our newly presented lunar IMP catalog and classification schemes also raise a list of outstanding questions concerning the nature and formation mechanism of lunar IMPs. Assessing these questions will solidify our knowledge of lunar thermal and geological evolution history.

Data Availability Statement

All original Lunar Orbiter photographs can be retrieved from the Lunar Orbiter Digitization Project (https://astrogeology.usgs.gov/Projects/LunarOrbiterDigitization/); all original Apollo photographs can be found at the Apollo Image Archive (http://apollo.sese.asu.edu/index.html); all original LRO data (LROC, LOLA, and SLDEM2015) are accessible at the PDS Geosciences Node (https://pds-geosciences.wustl.edu/missions/lro/default.htm), and all original Kaguya/SELENE TC and MI data are archived at SELENE Data Archive (https://darts.isas.jaxa.jp/planet/pdap/selene/). The updated IMP catalog and slope measurements of the various surface textures are accessible at Zenodo (https://zenodo.org/record/3772253).

Acknowledgments

This study is supported in part by the National Natural Science Foundation of China (nos. 41703063, 11941001, and 41972322), a Pre-research Project on Civil Aerospace Technologies no. D020205 funded by CNSA, the grant from Key Laboratory of Lunar and Deep Space Exploration, CAS (no. LDSE201902), the China Postdoctoral Science Foundation (nos. 2017M610421 and 2018T110682), and the Natural Science Foundation of Shandong Province (ZR2019MD008). J. W. H. gratefully acknowledges financial support from the NASA Lunar Reconnaissance Orbiter Lunar Orbiter Laser Altimeter (LOLA) experiment (grants NNX09AM54G and NNX11AK29G), and the NASA Solar System Exploration Research Virtual Institute (SSERVI) grant for Evolution and Environment of Exploration Destinations under cooperative Agreement no. NNA14AB01A at Brown University. L. W. thanks the Leverhulme Trust for support via an Emeritus Fellowship. We thank the Editors Laurent Montesi and David Baratoux and the reviewers for their very helpful comments.

References

Anderson, F. S., Whitaker, T. J., Wiesendanger, R., Wurz, P., Beck, S., & Levine, J. (2017). Revealing lunar history with CODEX: Miniature mass spectrometer Rb-Sr results. 5th European Lunar Symposium, University of Münster, Münster, Germany, 25-26

Anderson, J. A., Sides, S. C., Soltesz, D. L., Sucharski, T. L., & Becker K. J. (2004). Modernization of the integrated software for imagers and spectrometers. 35th Lunar and Planetary Science Conference, Lunar and Planetary Institute, League City, Texas, abstract #2039

Barker, M. K., Mazarico, E., Neumann, G. A., Smith, D. E., & Zuber, M. T. (2014). Merging digital elevation models from the lunar orbiter laser altimeter and Kaguya terrain camera. 45th Lunar and Planetary Science Conference. Lunar and Planetary Institute, The Woodlands, Texas, abstract #1635

Barker, M. K., Mazarico, E., Neumann, G. A., Zuber, M. T., Haruyama, J., & Smith, D. E. (2016). A new lunar digital elevation model from the lunar orbiter laser altimeter and SELENE terrain camera. *Icarus*, *273*, 346–355. https://doi.org/10.1016/j.icarus.2015.07.039

Bennett, K. A., Horgan, B. H. N., Bell, J. F., III, Meyer, H. M., & Robinson, M. S. (2015). Moon mineralogy mapper investigation of the Ina irregular mare patch. 46th Lunar and Planetary Science Conference, Lunar and Planetary Institute, The Woodlands, Texas, abstract #2646

Bowman-Cisneros, E. (2010). LROC EDR/CDR data product software interface specification. Retrieved from http://lroc.sese.asu.edu/data/LRO-L-LROC-2-EDR-V1.0/LROLRC_0001/DOCUMENT/LROCSIS.PDF

Braden, S. E. (2013). Analysis of spacecraft data for the study of diverse lunar volcanism and regolith maturation rates (Doctoral Dissertation). Retrieved from ASU Library. (http://repository.asu.edu/items/20943) Tempe, AZ: Arizona State University

Braden, S. E., Stopar, J. D., Robinson, M. S., Lawrence, S. J., van der Bogert, C. H., & Hiesinger, H. (2014). Evidence for basaltic volcanism on the Moon within the past 100 million years. *Nature Geoscience*, *7*(11), 787–791. https://doi.org/10.1038/ngeo2252

Carter, L. M., Hawke, B. R., Garry, W. B., Campbell, B. A., Giguere, T. A., & Bussey, D. B. J. (2013). Radar observations of lunar hollow terrain. 44th Lunar and Planetary Science Conference, Lunar and Planetary Institute, The Woodlands, Texas, abstract #2146

Cho, Y., Morota, T., Haruyama, J., Yasui, M., Hirata, N., & Sugita, S. (2012). Young mare volcanism in the Orientale region contemporary with the Procellarum KREEP Terrane (PKT) volcanism peak period ≒2 billion years ago. *Geophysical Research Letters*, *39*(11). https://doi.org/10.1029/2012GL051838

Donaldson Hanna, K. L., Evans, R., Bowles, N. E., Schultz, P. H., Greenhagen, B. T., & Bennett, K. A. (2016). Investigating young (<100 million years) irregular mare patches on the Moon using diviner observations. 47th Lunar and Planetary Science Conference, Lunar and Planetary Institute, The Woodlands, Texas, abstract #2127

Draper, D. S., Stopar, J. D., Lawrence, S. J., Denevi, B., John, K., Graham, L., et al. (2018). The Irregular Mare Patch Exploration Lander (IMPEL) SmallSat mission concept. 49th Lunar and Planetary Science Conference, Lunar and Planetary Institute, The Woodlands, Texas, Abstract #1617

El-Baz, F. (1972). New geological findings in Apollo 15 lunar orbital photography. Proceedings of 3rd Lunar and Planetary Science, 39–61

El-Baz, F. (1973). D-caldera: New photographs of a unique feature. In *Apollo 17 Preliminary Science Report* NASA SP-330, (pp. 3013–3017). Washington, DC: United States Government Printing Office.

Elder, C. M., Hayne, P. O., Bandfield, J. L., Ghent, R. R., Williams, J. P., Donaldson Hanna, K. L., & Paige, D. A. (2017). Young lunar volcanic features: Thermophysical properties and formation. *Icarus*, *290*, 224–237. https://doi.org/10.1016/j.icarus.2017.03.004

Evans, R. E., & El-Baz, F. (1973). Geological observations from lunar orbit. In *Apollo 17 Preliminary Science Report* NASA SP-330, (pp. 281–283). Washington, DC: United States Government Printing Office.

Garry, W., Robinson, M., Zimbelman, J., Bleacher, J., Hawke, B., Crumpler, L., et al. (2012). The origin of Ina: Evidence for inflated lava flows on the Moon. *Journal of Geophysical Research, Planets*, *117*(E12). https://doi.org/10.1029/2011JE003981

Garry, W. B., Hawke, B. R., Crites, S., Giguere, T., & Lucey, P. G. (2013). Optical maturity (OMAT) of Ina 'D-Caldera', the Moon. 44th Lunar and Planetary Science Conference, Lunar and Planetary Institute, The Woodlands, Texas, abstract #3058

Glaspie, L. M., Bennett, K. A., Gaddis, L. R., Donaldson Hanna, K. L., Horgan, B. H. N., Keszthelyi, L., et al. (2019). Characterization of a potential compositional halo around Ina irregular mare patch. 50th Lunar and Planetary Science Conference, Lunar and Planetary Institute, The woodlands, Texas, abstract #2889

Grice, J. P., Donaldson Hanna, K. L., Bowles, N. E., Schultz, P. H., & Bennett, K. A. (2016). Investigating young irregular mare patches on the Moon using Moon mineralogy mapper observations. 47th Lunar and Planetary Science Conference, Lunar and Planetary Institute, The Woodlands, Texas, abstract #2106

Haruyama, J., Hara, S., Hioki, K., Iwasaki, A., Morota, T., Ohtake, M., et al. (2012). Lunar global digital terrain model dataset produced from SELENE (Kaguya) terrain camera stereo observations. 43rd Lunar and Planetary Science Conference, Lunar and Planetary Institute, The Woodlands, Texas, abstract #1200

Haruyama, J., Matsunaga, T., Ohtake, M., Morota, T., Honda, C., Yokota, Y., et al. (2008). Global lunar-surface mapping experiment using the lunar imager/spectrometer on SELENE. *Earth, Planets and Space*, *60*(4), 243–255. https://doi.org/10.1186/BF03352788

Haruyama, J., Ohtake, M., Matsunaga, T., Morota, T., Honda, C., Yokota, Y., et al. (2009). Long-lived volcanism on the lunar farside revealed by SELENE terrain camera. *Science*, *323*(5916), 905. https://doi.org/10.1126/science.1163382

Head, J., & Gifford, A. (1980). Lunar mare domes: Classification and modes of origin. *The Moon and the Planets*, *22*, 235–258. https://doi.org/10.1007/BF00898434

Head, J. W., & Wilson, L. (2017). Generation, ascent and eruption of magma on the Moon: New insights into source depths, magma supply, intrusions and effusive/explosive eruptions (part 2: Predicted emplacement processes and observations). *Icarus*, *283*, 176–223. https://doi.org/10.1016/j.icarus.2016.05.031

Henriksen, M. R., Manheim, M. R., Burns, K. N., Seymour, P., Speyerer, E. J., Deran, A., et al. (2017). Extracting accurate and precise topography from LROC narrow angle camera stereo observations. *Icarus*, *283*, 122–137. https://doi.org/10.1016/j.icarus.2016.05.012

Hiesinger, H., Head, J. W., III, Wolf, U., Jaumann, R., & Neukum, G. (2006). New ages for basalts in Mare Fecunditatis based on crater size-frequency measurements. 37th Lunar and Planetary Science Conference. Lunar and Planetary Institute, The Woodlands, Texas, abstract #1151

Hiesinger, H., Head, J. W., Wolf, U., Jaumann, R., & Neukum, G. (2011). Ages and stratigraphy of lunar mare basalts: A synthesis. *Geological Society of America Special Papers*, *477*, 1–51. https://doi.org/10.1130/2011.2477(01)

Hiesinger, H., van der Bogert, C. H., Reiss, D., & Robinson, M. S. (2011). Crater size-frequency distribution measurements of Mare Crisium. 42th Lunar and Planetary Science Conference. Lunar and Planetary Institute, The Woodlands, Texas, abstract #2179

Hurwitz, D. M., Head, J. W., & Hiesinger, H. (2013). Lunar sinuous rilles: Distribution, characteristics, and implications for their origin. *Planetary and Space Science*, *79-80*, 1–38. https://doi.org/10.1016/j.pss.2012.10.019

Hurwitz, D. M., Head, J. W., Wilson, L., & Hiesinger, H. (2012). Origin of lunar sinuous rilles: Modeling effects of gravity, surface slope, and lava composition on erosion rates during the formation of Rima Prinz. *Journal of Geophysical Research, Planets*, *117*(E12). https://doi.org/10.1029/2011JE004000

Ivanov, M. A., Head, J. W., & Bystrov, A. (2016). The lunar Gruithuisen silicic extrusive domes: Topographic configuration, morphology, ages, and internal structure. *Icarus*, *273*, 262–283. https://doi.org/10.1016/j.icarus.2015.12.015

Jolliff, B. L., Gillis, J. J., Haskin, L. A., Korotev, R. L., & Wieczorek, M. A. (2000). Major lunar crustal terranes: Surface expressions and crust-mantle origins. *Journal of Geophysical Research, Planets*, *105*(E2), 4197–4216. https://doi.org/10.1029/1999JE001103

Lawrence, D. J., Elphic, R. C., Feldman, W. C., Prettyman, T. H., Gasnault, O., & Maurice, S. (2003). Small-area thorium features on the lunar surface. *Journal of Geophysical Research, Planets*, *108*(E9). https://doi.org/10.1029/2003JE002050

Lemelin, M., Lucey, P. G., Song, E., & Taylor, G. J. (2015). Lunar central peak mineralogy and iron content using the Kaguya multiband imager: Reassessment of the compositional structure of the lunar crust. *Journal of Geophysical Research, Planets*, *120*(5), 869–887. https://doi.org/10.1002/2014je004778

Masursky, H., Colton, G. W., & El-Baz, F. (1978). *Apollo over the Moon: A view from orbit (NASA SP-362)*. Washington, DC: Scientific and Technical Information Office.

Morota, T., Haruyama, J., Honda, C., Ohtake, M., Yokota, Y., Kimura, J., et al. (2009). Mare volcanism in the lunar farside Moscoviense region: Implication for lateral variation in magma production of the Moon. *Geophysical Research Letters*, *36*(21). https://doi.org/10.1029/2009GL040472

Morota, T., Haruyama, J., Ohtake, M., Matsunaga, T., Honda, C., Yokota, Y., et al. (2011). Timing and characteristics of the latest mare eruption on the Moon. *Earth and Planetary Science Letters*, *302*(3–4), 255–266. https://doi.org/10.1016/j.epsl.2010.12.028

Neish, C. D., Hamilton, C. W., Hughes, S. S., Nawotniak, S. K., Garry, W. B., Skok, J. R., et al. (2017). Terrestrial analogues for lunar impact melt flows. *Icarus*, *281*, 73–89. https://doi.org/10.1016/j.icarus.2016.08.008

Nelson, D. M., Koeber, S. D., Daud, K., Robinson, M. S., Watters, T. R., Banks, M. E., & Williams, N. R. (2014). Mapping lunar maria extents and lobate scarps using LROC image products. 45th Lunar and Planetary Science Conference. Lunar and Planetary Institute, The Woodlands, Texas, abstract #2961

Pasckert, J. H., Hiesinger, H., & van der Bogert, C. H. (2015). Small-scale lunar farside volcanism. *Icarus*, *257*, 336–354. https://doi.org/10.1016/j.icarus.2015.04.040

Pasckert, J. H., Hiesinger, H., & van der Bogert, C. H. (2018). Lunar farside volcanism in and around the south pole–Aitken basin. *Icarus*, *299*(supplement C), 538–562. https://doi.org/10.1016/j.icarus.2017.07.023

Qiao, L., Head, J., Wilson, L., Xiao, L., Kreslavsky, M., & Dufek, J. (2017). Ina pit crater on the Moon: Extrusion of waning-stage lava lake magmatic foam results in extremely young crater retention ages. *Geology*, *45*(5), 455–458. https://doi.org/10.1130/G38594.1

Qiao, L., Head, J. W., Ling, Z., & Wilson, L. (2019). Exploring a Sub-Classification Scheme for Irregular Mare Patches (IMPs), 50th Lunar and Planetary Science Conference, Lunar and Planetary Institute, The Woodlands, Texas, Abstract #2358

Qiao, L., Head, J. W., Ling, Z., Wilson, L., Xiao, L., Dufek, J. D., & Yan, J. (2019). Geological characterization of the Ina shield volcano summit pit crater on the Moon: Evidence for extrusion of waning-stage lava lake magmatic foams and anomalously young crater retention ages. *Journal of Geophysical Research, Planets*, *124*, 1100–1140. https://doi.org/10.1029/2018JE005841

Qiao, L., Head, J. W., Wilson, L., & Ling, Z. (2018). Lunar irregular mare patch (IMP) sub-types: Linking their origin through hybrid relationships displayed at Cauchy 5 small shield volcano. 49th Lunar and Planetary Science Conference. Lunar and Planetary Institute, The Woodlands, Texas, abstract #1392

Qiao, L., Head, J. W., Wilson, L., & Ling, Z. (2020). The Cauchy 5 small, low-volume lunar shield volcano: Evidence for volatile exsolution-eruption patterns and type 1/type 2 hybrid irregular mare patch (IMP) formation. *Journal of Geophysical Research, Planets*, *125*, e2019JE006171. https://doi.org/10.1029/2019JE006171

Qiao, L., Head, J. W., Xiao, L., Wilson, L., & Dufek, J. D. (2018). The role of substrate characteristics in producing anomalously young crater retention ages in volcanic deposits on the Moon: Morphology, topography, sub-resolution roughness and mode of emplacement of the Sosigenes lunar irregular Mare patch (IMP). *Meteoritics & Planetary Science*, *53*(4), 778–812. https://doi.org/10.1111/maps.13003

Robinson, M. S., Brylow, S. M., Tschimmel, M., Humm, D., Lawrence, S. J., Thomas, P. C., et al. (2010). Lunar reconnaissance orbiter camera (LROC) instrument overview. *Space Science Reviews*, *150*(1–4), 81–124. https://doi.org/10.1007/s11214-010-9634-2

Schultz, P. H. (1976). *Moon morphology*. Austin: University of Texas Press.

Schultz, P. H. (1991). The Moon: Dead or alive. In *Workshop on Mare Volcanism and Basalt Petrogenesis: "Astounding Fundamental Concepts (AFC)" Developed Over the Last Fifteen Years*, (pp. 45–46). Dallas, Texas: Lunar and Planetary Institute and Lunar and Planetary Sample Team (LAPST).

Schultz, P. H., Staid, M. I., & Pieters, C. M. (2006). Lunar activity from recent gas release. *Nature*, *444*(7116), 184–186. https://doi.org/10.1038/nature05303

Sim, C. K., Kim, S. S., Jeong, M., Choi, Y.-J., & Shkuratov, Y. G. (2019). Observational strategy for KPLO/PolCam measurements of the lunar surface from orbit. *Publications of the Astronomical Society of the Pacific*, *132*(1007), 015004. https://doi.org/10.1088/1538-3873/ab523d

Stooke, P. J. (2012). Lunar meniscus hollows. 43rd Lunar and Planetary Science Conference, Lunar and Planetary Institute, The Woodlands, Texas, abstract #1011

Stopar, J. D., Lawrence, S. J., Graham, L., Hamilton, J., Denevi, B., John, K. K., et al. (2019). Ina, Moon: Geologic setting, scientific rationale, and site characterization for a small planetary lander concept. *Planetary and Space Science*, *171*, 1–16. https://doi.org/10.1016/j.pss.2019.04.003

Strain, P. L., & El-Baz, F. (1980). The geology and morphology of Ina. In Proceedings of the 11th Lunar Science Conference (pp. 2437–2446)

Tye, A. R., & Head, J. W. (2013). Mare Tranquillitatis: Distribution of mare domes, relation to broad mare rise, and evidence of a previously unrecognized basin from LOLA altimetric data. 44th Lunar and Planetary Science Conference, Lunar and Planetary Institute, The Woodlands, Texas, abstract #1319

Tyrie, A. (1988). Age dating of mare in the lunar crater Tsiolkovsky by crater-counting method. *Earth, Moon, and Planets*, *42*(3), 245–264. https://doi.org/10.1007/BF00058489

Whitaker, E. A. (1972). An unusual mare feature, in Apollo 15 Preliminary Science Report NASA SP-289, pp. 2584–2585

Whitten, J., Head, J. W., Staid, M., Pieters, C. M., Mustard, J., Clark, R., et al. (2011). Lunar mare deposits associated with the Orientale impact basin: New insights into mineralogy, history, mode of emplacement, and relation to Orientale Basin evolution from Moon mineralogy mapper (M^3) data from Chandrayaan-1. *Journal of Geophysical Research, Planets*, *116*(E6). https://doi.org/10.1029/2010JE003736

Wilson, L., Hawke, B. R., Giguere, T. A., & Petrycki, E. R. (2011). An igneous origin for Rima Hyginus and Hyginus crater on the Moon. *Icarus*, *215*(2), 584–595. https://doi.org/10.1016/j.icarus.2011.07.003

Wilson, L., & Head, J. W. (2017a). Generation, ascent and eruption of magma on the Moon: New insights into source depths, magma supply, intrusions and effusive/explosive eruptions (part 1: Theory). *Icarus*, *283*, 146–175. https://doi.org/10.1016/j.icarus.2015.12.039

Wilson, L., & Head, J. W. (2017b). Eruption of magmatic foams on the Moon: Formation in the waning stages of dike emplacement events as an explanation of "irregular mare patches". *Journal of Volcanology and Geothermal Research*, *335*, 113–127. https://doi.org/10.1016/j.jvolgeores.2017.02.009

Wilson, L., & Head, J. W. (2018). Controls on lunar basaltic volcanic eruption structure and morphology: Gas release patterns in sequential eruption phases. *Geophysical Research Letters*, *45*(12), 5852–5859. https://doi.org/10.1029/2018GL078327

Yue, Z., Li, W., Di, K., Liu, Z., & Liu, J. (2015). Global mapping and analysis of lunar wrinkle ridges. *Journal of Geophysical Research, Planets*, *120*, 978–994. https://doi.org/10.1002/2014JE004777

Zhang, F., Zhu, M. H., Bugiolacchi, R., Huang, Q., Osinski, G. R., Xiao, L., & Zou, Y. L. (2018). Diversity of basaltic lunar volcanism associated with buried impact structures: Implications for intrusive and extrusive events. *Icarus*, *307*, 216–234. https://doi.org/10.1016/j.icarus.2017.10.039